TRIBHUVAN UNIVERSITY
INSTITUTE OF ENGINEERING
PULCHOWK CAMPUS

THESIS NO: PUL078MSGtE014

Numerical Investigation of Effect of Compaction on Serviceability Behavior of Geosynthetic Reinforced Structures

by

Saurav Ghimire

A THESIS
SUBMITTED TO THE DEPARTMENT OF CIVIL ENGINEERING
IN PARTIAL FULFILLMENT OF THE REQUIREMENTS FOR THE
DEGREE OF MASTER OF SCIENCE IN
GEOTECHNICAL ENGINEERING

DEPARTMENT OF CIVIL ENGINEERING
LALITPUR, NEPAL

DECEMBER, 2023

Copyright

TRIBHUVAN UNIVERSITY

INSTITUTE OF ENGINEERING

PULCHOWK CAMPUS

DEPARTMENT OF CIVIL ENGINEERING

PULCHOWK, LALITPUR

Approval page

The undersigned certify that they have read, and recommended to the Institute of Engineering for acceptance, a thesis entitled, " **Numerical Investigation of Effect of Compaction on Serviceability Behavior of Geosynthetic Reinforced Structures**" submitted by Mr. Saurav Ghimire (078/MSGtE/014) in partial fulfillment of the requirement for the degree of Master of Science in Geotechnical Engineering.

..…..……

Supervisor: Dr. Santosh Kumar Yadav

Department of Civil Engineering

Institute of Engineering, Pulchowk Campus

…….……

External Examiner: Er. Bharat Bahadur Dhakal

Department of Civil Engineering

Institute of Engineering, Pulchowk Campus

..…..……

Program Coordinator: Dr. Santosh Kumar Yadav

Department of Civil Engineering

Institute of Engineering, Pulchowk Campus

December 2023

Abstract

Geosynthetic Reinforced Structures (GRS) play a pivotal role in various construction applications, serving as reinforced retaining structures, bridge abutments, and slope stabilizers. The technology employs geotextile or geogrids in backfill layers to develop tensile strength through friction and interlocking with the soil, minimizing settlement issues. GRS mechanisms involve apparent cohesion development, increased confining pressure, and potential soil dilatancy suppression. Research on GRS behavior encompasses factors like reinforcement spacing, stiffness, compaction effects, facing rigidity, and seismic behavior.

This study addresses a gap in understanding the impact of compaction load on lateral wall deformation during the serviceability stage. Utilizing Finite Element Method (FEM) 2D, the numerical model investigates compaction load effects on lateral wall deformation and reinforcement axial strain. Experimental findings underscore the influence of backfill compaction on soil stiffness and deformation reduction. Parametric analysis reveals compaction's substantial role in resisting lateral deformation, with decreased vertical reinforcement spacing and increased axial stiffness correlating with diminished lateral wall deformation. The study emphasizes that heavy compaction effectively mitigates both vertical and lateral deformation induced by traffic loads. Field modeling of a Geosynthetic Reinforced Bridge abutment validates these findings, showcasing the practical significance of compaction in enhancing the performance of GRS structures.

Acknowledgements

I wish to express my deepest and sincere appreciation to my supervisor and program Co-ordinator Dr. Santosh Kumar Yadav for giving me a unique opportunity to work on such an important topic. His continuous guidance, encouragement and critical suggestion throughout the course of this study are greatly acknowledged. I consider myself fortunate to work under his supervision.

I would like to acknowledge all the faculty members of Department of Civil Engineering for the knowledge and concepts they gave me during my study at IOE, Pulchowk Campus.

I am equally thankful to my friends MSGtE078 batch for their cooperation and intellect suggestions. My sincere thanks also go to all those who gave valuable support, critical comments, suggestions and advice on different stages of my research work.

Last but not the least, I would like to start off by thanking my parents for their persuasion and continuous support throughout my academic perseverance. They were always there cheering me up and stood by me through good and bad times, which motivated me to overcome the difficulties and led to this stage of my thesis.

Saurav Ghimire
078/MSGTE/014
December 2023

List of Tables

List of Figures

List of abbreviations

c_r: Apparent Cohesion

CIS: Compaction Induced Stress

CSSM: Critical State Soil Mechanics

E_{50}^{ref} : Reference secant stiffness from drained triaxial test

E_{ur}^{ref}: Reference unloading/reloading stiffness

EOC - End of Construction

FEM: Finite Element Method

FLAC: Fast Lagrangian Analysis of Continua

GRS - Geosynthetic Reinforced Soil

GRS-BA - Geosynthetic Reinforced Soil Bridge Abutment

GRS-IBS - Geosynthetic Reinforced Soil Integrated Bridge System

HSM: Hardening Soil Model

IRC: Indian Road Congress

MSE: Mechanically Stabilized Earth

PCS - Post Construction Surcharging

RD: Relative Density

RSF: Reinforced Soil Foundation

SGC: Soil Geosynthetic Composite

UDL - Uniform Distributed Load

Φ: Frictional Angle

$\emptyset$: Dilatancy angle

R_f :Failure ratio

1. INTRODUCTION

1.1. Background

Geosynthetic Reinforced Soil (GRS) Structure has been used as the various infrastructure projects which includes the use of GRS structure as retaining walls for slopes, embankment for roads and recently GRS technology has been used as replacement of rigid concrete bridge abutment. Geosynthetic Reinforced Soil Bridge abutment (GRS – BA) has been used as load bearing structure for carrying concentrated traffic loads. The main use of GRS-BA has been used in Elevated Structure as well as with the use of scouring counter measures, it has been used for drainage crossing.

GRS Bridge Abutment technology has been used as Geosynthetic Reinforced Soil Integrated Bridge System (GRS – IBS) as well as GRS -BA. The former uses the integrated road approach connected to the bridge deck The Primary objective of using GRS Bridge Abutment is to counter the bump problem induced due to differential settlement of backfill soil and more rigid concrete abutment. The use of GRS – BA as replacement of concrete abutment not only expedite the construction period but also reduces the cost of construction of structure.

Numerous studies focusing on the backfill material, reinforcing structure, facing element and foundation soil characteristics has been conducting for determining the influencing parameters for the performance of the GRS system. The study involves testing of prototypes, full scale testing, analytical modelling and numerical modelling for prediction of the performance of the system. Among various studies, study of the effect of the backfill compaction on End of Construction (EOC) and Post Construction Surcharging (PCS) has been done in limited number. The effect of vibratory roller compaction has been idealized as uniform distributed load (udl) while performing the numerical simulations. The effect of the modelling the compaction effort, load on PCS has been studied in this research work.

1.2. Problem Statement

The difference in rigidity between backfill and abutment causes the differential settlement and creating bump problems at the approach of the bridge, which can be mitigated using various methods. Among which use of the GRS-BA has been adopted for low, bread and butter type of bridges in various countries. Several design guidelines

have been utilized for the design and construction. The structural stability and limit state of serviceability demands 2% of lateral strain of wall facing, which can be restricted if the compaction induced stress is considered. The effect of the different compaction efforts on the long-term behavior or behavior subjected to the service loads has been considered rarely. So, in this study, after verification of the experimental and full-scale field test, the effects of the compaction on restricting the deformation during the application of service load is studied using finite element method and also due to the compaction. Hence, two models, one experimental geosynthetic reinforced wall and another full-scale field mode has been considered for the study.

1.3. Objective

The main objectives of the study are:

1. Validate an existing numerical model of Geosynthetic Reinforced Soil Structures by comparing it to relevant literature and experimental data.
2. Analyze the influence of compaction loads on the deformation behavior of Geosynthetic Reinforced Soil Structures both during construction and in the post-construction phase.
3. Analyze how the variation in compaction load, soil properties, reinforcement properties affect the deformation behavior of Geosynthetic Reinforced Soil Structures.
4. Analyze the use of GRS structure as bridge abutment and understand the performance of structure subjected to traffic loads.

1.4. Scope and Limitation of study

The study fully focused on the numerical investigation of the effect of backfill compaction on field model and experimental model. Hence, the study is limited to the numerical simulation and a experimental prototype can be made for studying the real field behavior of the structure.

The research is only limited to the two-dimensional plain strain finite element analysis of the structure. Hence, following list elaborates the limitations of this study:

1. Model was prepared only on plain strain condition which limits the three-dimensional effect and effect of the aperture of the geogrid.

2. Backfill compaction is compacted using a common uniformly distributed load, which in real life is different process of application.

2. LITERATURE REVIEW

2.1. Introduction to Geosynthetic Reinforced Soil Structure

Soil mass is strong in the compression and shear as compared to the tension. The weak tensile property of soil mass can be improved by providing the reinforcement which creates bond between soil mass and reinforcement and provides tensile property for soil mass subjected to tensile stress. Also, the inclusion of the soil reinforcement in soil mass increases the stiffness, strength, confinement, reduces lateral deformation and reduces tendency for soil dilatancy. In Geosynthetic Reinforced Structure (GRS), geosynthetics are commonly used as reinforcing element which are sandwiched between the soil layers. The vertical spacing between the reinforcement layers are typically less than 12 inches (VanBuskirk, 2010).

2.1.1. Difference between GRS and MSE Walls

The Geosynthetic Reinforced Soil (GRS) Structure has been emerged as the alternative solution for ground-up earth retention for which the use of Mechanically Stabilized Earth (MSE) walls have been used for years. MSE walls are mainly used for the earth retention structure and are common in highway structures. The recent development of GRS structure enables agencies to adopt the structure as bridge abutment for level crossings and drainage crossings.

GRS are different from traditional MSE walls in two unique ways:

1. Closely spaced layers (typically less than 12 inches) that provide reinforcement to the soil mass (VanBuskirk, 2010).
2. Internal reinforcement is frictionally attached to the facing material while the connection of the reinforcement and facing element is done mechanically in MSE walls.

Also, the use of closely spaced tensile inclusion in horizontal layers of the fill material enables to achieve stability of a soil mass which results in the low failure rate in GRS walls in comparison to MSE walls (Wu, 2019).

A well-documented difference between GRS and MSE walls can be illustrated by the Figure 2.1 which shows the failure mechanism for reinforced structure with different reinforcement spacings. For vertical reinforcement spacing less than 8 inches, a shear surface formed through the composite, leading to rupture of reinforcement concluding

the full tensile strength of reinforcement was mobilized while in spacing larger than 8 inches, the same mode of failure was not observed; the failure was soil failure between the sheets of the reinforcement where the tensile strength of reinforcement was not fully mobilized. This concludes the use of close vertical spacing of reinforcement allows to form soil composite which is internally stable and the use of facing element is for the façade purpose unlike MSE walls where the facing elements are structural units.

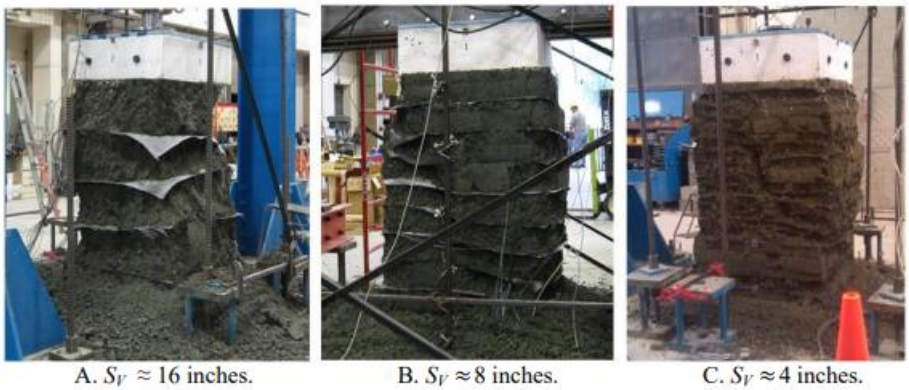

Figure 2.1 Failure behavior of GRS versus MSE as shown in tests conducted at reinforcement spacings of 16, 8, and 4 inches (M. Adams et al., 2018).

2.2. Design Criteria

In accordance with Federal Highway Authority (FHWA) guidelines, the permissible vertical strain deformation in the GRS-BA abutment should not exceed 0.5% of the abutment height. To determine the maximum lateral deformation at the face, one can employ the assumption of composite behavior in a properly constructed GRS-BA mass, where both reinforcement and soil strain laterally extend in unison (M. Adams et al., 2018). Under the assumption of no change in volume of the GRS-BA abutment due to vertical loading, (M. Adams et al., 2018) specifies that the lateral strain is twice the vertical strain, necessitating it to be limited to less than 1% of the abutment height.

2.3. Geosynthetic Reinforced Soil abutment structure

Geosynthetic Reinforced Soil (GRS) Bridge Abutment, termed as GRS-BA, have close reinforcement spacing which helps in improvement of bearing capacity to support bridge load. GRS abutment is made from the backfill and close spacing of the geogrid and geotextile. The locally available backfill material and the low-cost geogrids or geotextiles lowers the construction cost. Recently, GRS -IBS have been developed in which (Saghebfar et al., 2017) found that the bump problem is reduced as both bridge

structure and approach backfill settle together. Both GRS abutment and GRS – IBS are of lesser construction cost and environmentally friendly.

The carbon emissions produced by traditional concrete bridge abutment can be reduced by the introduction of GRS- BA and GRS – IBS technology (M. T. Adams et al., 2007). As this technology does not require highly skilled manpower and sophisticated equipment, the technology can save, up to 20% in construction cost and construction time period as compared to concrete abutment. (M. T. Adams et al., 2007). The relative cost analysis is also conducted by (Jelušič & Zlender, 2021) in Serbia and found the cost can be reduced by 20%.

The development of the GRS abutment started in the early 1970's. The US forest service constructed wall in steep hilly terrain (Zelenko et al., 2019). FHWA introduced GRS-IBS structure in the early 2000's as aim to facilitate smooth transition between bridge deck and the roadway and to replace old broken bridges (Zelenko et al., 2019). Being environmentally friendly and having lower construction cost, GRS abutments have been interest of practitioners and the researchers. Research on the performance of the structure, properties of the structure have been conducted using both experimental and numerical methods. A typical GRS-IBS consists of following components (M. Adams et al., 2018):

1. Beam seat: To support the bridge superstructure and supported directly on the bearing zone of thickness 0.2- 0.3m.
2. Facing elements such as modular concrete block, cast in place wall, rigid face. The facing element is frictionally connected to the geosynthetic layer.
3. Reinforced integrated approach (RIA) which is jointless structure connected to the bridge structure.
4. Bearing bed with reinforcement to support bridge load with more vertical spacing.
5. Granular backfilled geosynthetic reinforced soil (GRS) abutment to support all loads and bridge sill with normal spacing of reinforcement.
6. Reinforced soil foundation (RSF) to increase the load bearing capacity of the GRS abutment.
7. Rip Rap to protect the GRS- BA from the scour.

For the design and construction guidelines of geosynthetic reinforced bridge abutment, the guideline of Federal Highway Administration (FHWA) can be referenced (M. Adams et al., 2018). where the recommended abutment height and span length are respectively not more than 9.1m and 42.7m.

2.4. Mechanics of Geosynthetic Reinforced Soil Structure

The bonding between the soil mass and the reinforcement enables the strain developed in the mass of soil to generate the reinforcement strain which provides the tensile strength to the soil mass. The mechanisms by which the reinforcement increases the soil strength and stiffness are subsequently described in the following sub headings.

2.4.1. Concept of apparent cohesion

It was observed that the inclusion of a reinforced layer leads to an increase in the principal stress at failure, accompanied by an apparent cohesion (Yang, 1972) . Furthermore, the study demonstrated that the frictional angle (Φ) values remain unchanged, provided that there is no slippage occurring at the soil-reinforcement interface. The apparent cohesion (c_r) of composite soil reinforced structure based on (Schlosser & Long, 1974) involves following equation:

$$c_r = T_f . \frac{\sqrt{Kp}}{2.Sv} + c \qquad (1)$$

Where T_f: the tensile strength; Sv: is the vertical spacing of the reinforcement; Kp: the coefficient of Rankine passive earth pressure; and c: cohesion of soil.

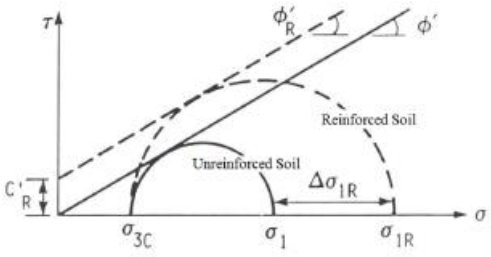

Figure 2.2 Concept of apparent Cohesion due to the presence of Reinforcement (Schlosser & Long, 1974)

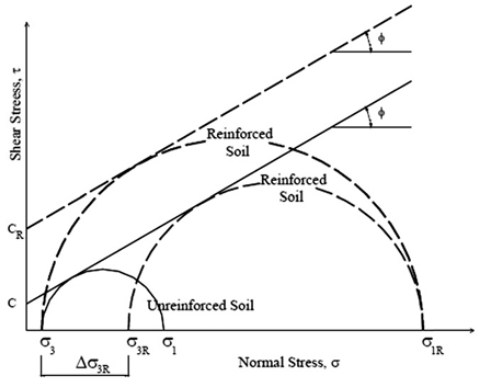

Figure 2.3 Concepts of apparent cohesion and apparent confining pressure of a soil-geosynthetic composite(Wu & Pham, 2013)

2.4.2. Concept of increase of apparent confining pressure

The idea of an increase in apparent confining pressure is another way to describe how reinforced soil works. According to this theory, an increase in confining pressure leads to an increase in the axial strength of reinforced soil.

2.4.3. Concept of Suppression of Soil Dilation

When under shear stress, loose granular soil shrinks. Soil particles fall into the spaces between them as a result of the shear stress, which causes the soil to compress. On the other hand, when dense granular soil is under shear stress, its volume increases. The phenomenon of stress-strain behavior and also the volume change behavior of unreinforced and reinforced compacted fill material is shown by the curve in Figure 2.4 and Figure 2.5. Before volumetric strain in granular material achieves its maximum compressive volumetric strain, there often is a little contraction. The volume of the soil sample then grows as particles move past one another and produce dilatation.

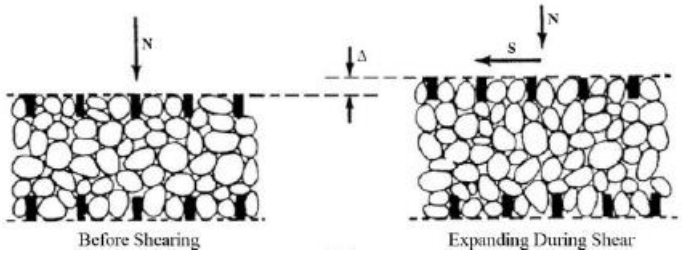

Figure 2.4 Volume Change Behavior of Compacted unreinforced Granular Soil (Wu et al., 2014).

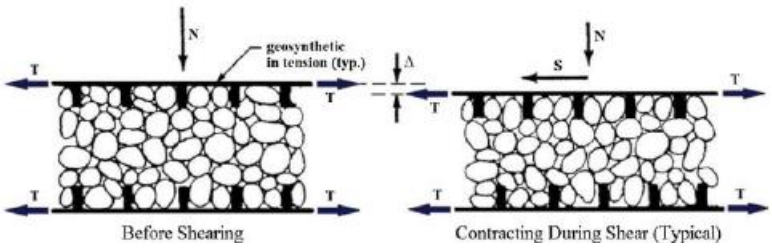

Figure 2.5 Volume Change Behavior of Compacted reinforced Granular Soil (Wu et al., 2014)

Reinforcement can prevent soil from expanding. Through friction at the soil-reinforcement interface, tensions in the soil mass cause the reinforcements to tensile strain and stretch. Stretched geosynthetics create contained borders that tend to prevent soil expansion. The mechanism of suppression of dilation is presented in Figure 2.6

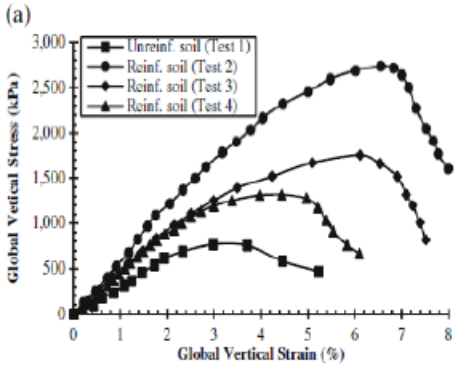

Figure 2.6 Stress - Strain Behavior of unreinforced and reinforced soil mass(Wu et al., 2014)

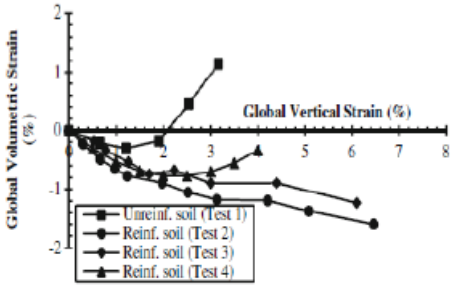

Figure 2.7 Volume Change Behavior of unreinforced and reinforced soil mass (Wu et al., 2014)

2.5. Concept of Compaction Induced Stress

An extra vertical load on a soil mass will often cause both vertical and horizontal strains inside the soil mass to increase. The rise in horizontal stress may only be marginally reduced if the addition of downward vertical load is later eliminated, whereas the increase in z directional stress, z being vertical, would decrease to almost nothing. The term "lock-in" lateral stress refers to the net increase in horizontal stress that "remained" in the soil mass. Fill compaction occurs when there is an increase in vertical load and its subsequent reduction during the construction of GRS mass. Here, "Compaction-Induced Stress" (CIS) is the term used to describe the "lock-in" lateral stress resulting from such compaction (Gui et al., 2020a).

(Gui et al., 2020a) conducted a series of numerical analyses of a hypothetical 6 m high geosynthetic reinforced soil (GRS) mass and a 2 m high soil geosynthetic composite (SGC) mass was carried out. Through the simulation of the SGC mass and comparison with experimental lateral displacements and reinforcement strains, the impact of simulated compaction techniques, compaction loads, and surcharge loads has been studied. The compaction process resulted in the development of the so-called compaction-induced stress (CIS), which subsequently increases the stiffness and strength of the fill material.

Similarly, (Mirmoradi & Ehrlich, 2015) proposed a new simple analytical procedure (AASTHO modified) which considers the effects of compaction induced stress. The procedure is based on the equation suggested by (Wu & Pham, 2010) to calculate increase in lateral stress in a reinforced soil mass due to compaction. Author also conducted two numerical analyses for modelling of compaction (one with two distributed loads at the top and the bottom of each layer and one with a distributed load only at top of each soil layer). The analytical method and numerical procedure with distributed load at top and bottom of each layer, results the values of maximum reinforcement tension, that agrees with that from full-scale test and those calculated by (Ehrlich & Mitchell, 1994). The numerical procedure involving use of a distributed load only at top of each soil layer overestimates the maximum reinforcement tension.

Examinations of case study outcomes and numerical and physical modeling of reinforced soil structures revealed that compaction might play a key role in releasing tension in the reinforcements and minimizing movements after construction. The

findings demonstrated that the lowering of the soil void ratio is not the only way that soil compaction occurs. Compaction can also result in a notable rise in the horizontal stress inside the reinforced soil mass and produce a material that is somewhat over consolidated.

2.6. Numerical Simulation of Compaction Induced Stress

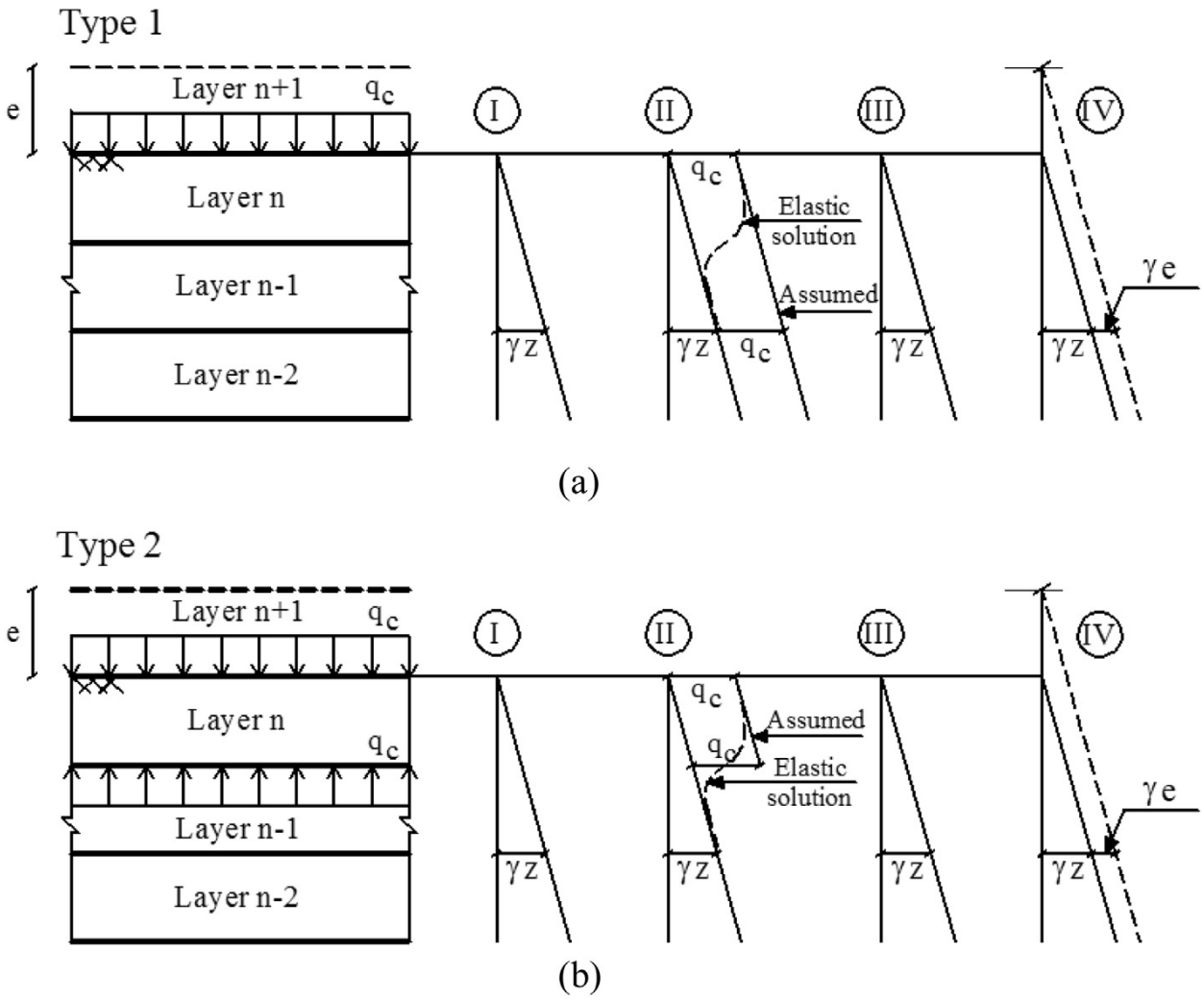

Figure 2.8 Modelling of compaction (Mirmoradi & Ehrlich, 2015)

(Ehrlich et al., 2012a, 2012b; Mirmoradi & Ehrlich, 2015) provided modelling of compaction induced stresses using two methods:

1. A uniform vertical stress as uniformly distributed load applied to the top each backfill soil as the wall was modelled from bottom of each soil layer.

2. A uniform vertical stress as uniformly distributed applied to the top and bottom of each backfill soil as the wall was modelled from bottom of each soil layer.

(Ehrlich et al., 2012a, 2012b; Mirmoradi & Ehrlich, 2015) method 1 overestimates the performance characteristics and results from method 2 satisfies the experimental results.

Figure 2.8 shows two different methods for the numerical simulation of the compaction induced stress due to backfill compaction. When compared to the dashed line depicted by the elastic solution, the curves corresponding to the compaction modeling employing process type 2 appear to more accurately represent the vertical stress actually created during roller operation.

For the staged construction, the process involves the placement of soil layer, compaction of soil layer placed, and placement of the next soil layer at the end of compaction of previous layers.

2.7. Numerical studies

Conducting a parametric investigation using sophisticated instruments is capital intensive, hectic and time consuming. In recent years with the development of the computational powers, the experiments can be conducted using numerical analysis. A number of researchers uses numerical modelling techniques to investigate the effect of parameters of GRS BA on its performance. The validated the numerical model with the physical full scale or reduced scale experiments are the used to simulate the behavior of the system by changing the parameters.

The numerical modelling techniques uses the differential equations and boundary value problem and converts them into the linear algebraic equations. The numerical modelling can be used using finite element method and finite difference method. The discretization in FEM involves the breaking the large system into smaller finite mesh upon which the numerical procedures are performed. The solution of partial differential equation in FDM are obtained by approximating PDEs into difference equation. Both FDM and FEM are useful for solving wide range of problems in geotechnical engineering and can be used for solving time dependent and non-dependent, linear and nonlinear problems. In geotechnical engineering, commercial software FLAC uses FDM approach while FEM can be solved using opensees, Plaxis 2D and 3D. Authors like (Abdelouhab et al., 2011; M. Abu-Farsakh et al., 2018a, 2018b; M. Y. Abu-Farsakh et al., 2019; Ardah et al., 2017; Askari et al., 2021; Gui et al., 2020a, 2020b; Huang et al., n.d.; Rowe & Skinner, 2001; Zheng & Fox, 2017) conducted numerical analysis to

understand static and seismic performance of GRS- BA. The nonlinear and irreversible behavior of soil can't explicitly be described using MC model. So, the researchers have been using more advance soil models like soft soil model, MCC model, Duncan-Chang, Cap Yield , HYP, Hardening Soil and Hardening Soil with small strain model. (Huang et al., n.d.) studied the effect of using three different constitutive soil models. The author uses a finite difference (FLAC) model in which backfill sand was modelled using three different constitutive model: linear elastic-plastic Mohr- Coulomb, Duncan-Chang hyperbolic model and Lade's single hardening model. Influence of constitutive models were compared with the experimental results like toe footing loads, foundation pressures, facing displacements, connection loads, and reinforcement strains.

In finite element analysis, geosynthetic can be modelled as Linear Elastic perfectly plastic while in finite difference software, the geosynthetic is modelled as Linear Elastic beam element. In 2D plain strain FE analysis, geosynthetic can be modelled as special tension 5-noded elements to describe the axial forces (Ardah et al., 2017). For modelling the interface, it can be modelled as Linear elastic with Mohr Coulomb failure and Cable element in Plaxis 2D or 3D and FLAC respectively.

Numerical model is performed to investigate effects of different parameters and variables, which is not viable to conduct on typically costly physical model test. The two-dimensional and three-dimensional numerical analysis are conducted to study the effects of different parameters. The three-dimensional Finite element (FE) analysis was performed for different loading cases and it was predicted that the maximum lateral deformation at face was more during abnormal case than the under-service loading (M. Abu-Farsakh et al., 2018a). Not much differences in the results were obtained between 3D and 2D FE numerical analysis and the FHWA analytical method over predicts the results by 1.5 to 2.5 times higher than that predicted by FE analysis (M. Abu-Farsakh et al., 2018a).

2.7.1. Finite Element Model

Finite Element Modeling (FEM) is a powerful numerical technique used in engineering and physics to simulate and analyze complex structures and physical phenomena. It is particularly prevalent in the field of structural and mechanical engineering, providing a versatile and effective approach for solving problems related to stress, heat transfer, fluid dynamics, and other physical behaviors.

Key aspects of Finite Element Modeling include:

1. Discretization: FEM divides a complex geometry or physical domain into smaller, simpler subdomains called elements. These elements collectively cover the entire structure, and their interactions are analyzed to understand the overall behavior of the system.

2. Nodes and Elements: Nodes are points where the physical quantities of interest (such as displacement, temperature, or stress) are calculated. Elements are the geometric shapes that connect nodes and define the local behavior of the material within the structure.

3. Mathematical Representation: FEM employs mathematical equations to represent the physical behavior of materials and structures. These equations are typically derived from fundamental principles such as equilibrium, compatibility, and material constitutive relations.

4. Assembly of System Equations: The system equations are assembled by combining the individual element equations based on the connectivity of nodes. This results in a system of algebraic equations that represents the entire structure.

5. Solution Techniques: Various numerical methods, such as the matrix method or iterative solvers, are employed to solve the system equations. These techniques provide numerical approximations for the behavior of the system under given conditions.

6. Applications: Finite Element Modeling is widely applied in diverse engineering disciplines, including structural analysis, heat transfer, fluid dynamics, electromagnetics, and geotechnical engineering. It is used to predict how structures will respond to different loading conditions, optimize designs, and understand the effects of various parameters.

7. Software Tools: Several specialized software tools, such as ANSYS, Abaqus, and COMSOL, facilitate the implementation of Finite Element Modeling. These tools offer user-friendly interfaces for creating models, defining material properties, applying loads and constraints, and visualizing results.

Finite Element Modeling has become an integral part of the engineering design and analysis process, enabling engineers to simulate and understand complex behaviors before physical prototypes are constructed. Its versatility and accuracy make it a valuable tool in various industries for optimizing designs, ensuring structural integrity, and improving overall performance.

2.7.2. Constitutive Models

Soil constitutive modeling, a specialized branch of geotechnical engineering, is dedicated to comprehending and forecasting the mechanical responses of soil under diverse loading and environmental conditions. The term "constitutive" pertains to the connection between stress and strain within a material, and these models aim to mathematically articulate such relationships for soil.

Soils manifest intricate mechanical behaviors influenced by factors like particle interactions, water content, stress history, and the presence of additional materials. Constitutive models strive to encapsulate these intricacies, furnishing a framework to predict soil reactions under various loading scenarios. Their significance extends to the design of foundations, slopes, retaining structures, and other geotechnical engineering applications.

A spectrum of constitutive models exists, ranging from basic empirical models to sophisticated mathematical formulations grounded in soil mechanics principles. These models consider variables such as soil type, stress state, strain rate, and temperature, providing a holistic understanding of soil behavior. Prominent examples encompass the Mohr-Coulomb model, Cam-Clay model, Hardening Soil Model, and critical state soil mechanics models.

The deployment and refinement of constitutive models in soil mechanics play a pivotal role in refining the precision of geotechnical analyses, augmenting the safety, and efficiency of civil engineering projects. Researchers and practitioners continually enhance these models to better portray the intricate behavior of soils across diverse conditions, contributing to ongoing advancements in the field of geotechnical engineering.

Noteworthy categories of constitutive models include:

A. Elastic Models: These presuppose linearly elastic soil behavior, with stress and strain exhibiting a linear relationship. Examples include linear elastic and nonlinear elastic models.

B. Plastic Models: Focused on plastic deformations, these models often incorporate yield surfaces, delineating the upper boundary for plastic deformation. Examples include the Cam-Clay model and Modified Cam-Clay model.

C. Elastoplastic Models: Combining aspects of both elastic and plastic behavior, these models account for plasticity at higher strains and elasticity at smaller strains. The Mohr-Coulomb model is a popular elastoplastic model.

D. Critical State Models: Grounded in the concept of critical state, denoting the condition of maximum density and shear strength, these models are applied to sands and gravels to represent soil behavior around the critical state.

2.7.2.1. Mohr-Coulomb model

The Mohr-Coulomb model is a widely used constitutive model in geotechnical engineering to describe the stress-strain behavior of soils. Developed independently by engineers Mohr and Coulomb, this model provides a simple yet effective representation of soil mechanics, particularly in the context of soil shear strength.

Key features of the Mohr-Coulomb model include:

1. Shear Strength: The model focuses on capturing the shear strength of soils, representing the maximum shear stress a soil can sustain before failure occurs. The shear strength is defined by two parameters: cohesion (c) and angle of internal friction (φ).
2. Cohesion (c): Represents the cohesive forces between soil particles. It is the intercept on the shear stress axis when the normal stress is zero.
3. Angle of Internal Friction (φ): Describes the resistance to particle movement due to friction between soil particles. It is the slope of the Mohr-Coulomb failure envelope.
4. Failure Envelope: The Mohr-Coulomb failure criterion is typically represented as an envelope in the principal stress space. For a given normal stress (σ) and shear stress (τ), failure occurs when the state of stress reaches or exceeds the failure envelope.

5. Applicability: The model is applicable to both cohesive and cohesionless soils. For cohesive soils, the cohesion term becomes significant, while for cohesionless soils, the angle of internal friction dominates.
6. Assumptions: The Mohr-Coulomb model assumes that soil failure is controlled by a combination of cohesive and frictional forces and that failure occurs along a well-defined failure plane.
7. Limitations: While the Mohr-Coulomb model is widely used, it has limitations. It does not account for strain-softening or strain-hardening behavior, and it assumes that shear strength is independent of the normal stress.

The simplicity of the Mohr-Coulomb model makes it suitable for many engineering applications, such as slope stability analysis, foundation design, and earth pressure calculations

2.7.2.2. Hardening Soil Model

The Hardening Soil Model (HSM) is a constitutive model used in geotechnical engineering to describe the stress-strain behavior of soils. This model is particularly well-suited for capturing the complexities of soil response under different loading conditions, making it valuable for analyzing soil behavior in various geotechnical applications.

Key features of the Hardening Soil Model include:

1. Isotropic Hardening: The model incorporates isotropic hardening, meaning it considers the increase in the yield surface size as the soil undergoes plastic deformation. This feature allows the model to account for the plastic strain accumulation in response to loading.
2. Critical State Soil Mechanics: The Hardening Soil Model is often associated with Critical State Soil Mechanics (CSSM), a framework that describes soil behavior at a critical or ultimate state. CSSM provides a theoretical basis for understanding soil deformation and strength characteristics, and the Hardening Soil Model incorporates these principles into its formulation.
3. Stress-Strain Relationships: The model defines stress-strain relationships by considering both elastic and plastic deformations. It accounts for the initial elastic modulus, yielding behavior, and post-yield soil hardening.

4. Loading and Unloading Paths: The Hardening Soil Model is capable of simulating different loading and unloading paths, making it versatile for analyzing cyclic loading scenarios or changes in stress conditions.
5. Versatility: This model can be applied to a wide range of soil types, making it suitable for various geotechnical engineering applications, including slope stability analysis, foundation design, and tunneling.

The elastoplastic hardening soil model (HSM) is used to simulate the nonlinear behavior of the soil (backfill). The principle of plasticity served as the foundation for the development of the hardening soil. In this model, the total stresses are calculated using a stress-dependent stiffness that is variable for loading and unloading/reloading. Depending on the volumetric and shear strains of the plastic, an isotropic hardening is postulated. When it comes to frictional hardening, a non-associated flow rule is assumed and an associated flow rule when it comes to cap hardening.

(Schanz et al., 1999) explained the formulation and validation of hardening soil model in brief. A hyperbolic curve is assumed for the strain-stress relationship for the primary loading stress path. The hyperbolic function, as given by (Kondner & Zelasko, 1963)for the drained triaxial test can be formulated as:

$$\varepsilon_1 = \frac{q_a}{2E_{50}} \frac{q}{q_a - q}, \text{for} q < q_f \tag{1}$$

where $\varepsilon 1$ is the axial strain, and q is the deviatoric stress. The ultimate deviatoric stress (qf) is defined as:

$$q_f = \frac{6 \sin \emptyset'}{3 - \sin \emptyset'} (\sigma_3' + c' \cot \emptyset') \tag{2}$$

and the quantity (q_a) is

$$q_a = \frac{q_f}{R_f} \tag{3}$$

where q_f : the ultimate deviatoric stress at failure, which is derived from the Mohr–Coulomb failure criterion involving the strength parameters c' and $\emptyset'$.

q_a : the asymptotic value of the shear strength and R_f: the failure ratio.

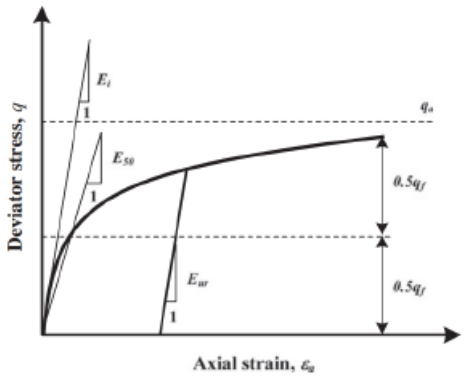

Figure 2.9 A hyperbolic curve for primary loading stress path for a standard triaxial test (Schanz et al., 1999)

Table 2.1 Hardening Soil Input Parameters

Parameter	**Description**
$\emptyset'$	Internal friction angle
c'	Cohesion
R_f	Failure ratio
$\emptyset$	Dilatancy angle
E_{50}^{ref}	Reference secant stiffness from drained triaxial test
E_{ur}^{ref}	Reference unloading/reloading stiffness
m	Exponential Power
ϑ_{ur}	Unloading/reloading Poisson's ratio
k_o^{nc}	Coefficient of earth pressure at rest

The non-linear stress- strain behavior of the soil and rock mass for primary loading demands the stress dependent stiffness modulus rather than the average stiffness modulus used in Mohr Coulomb model. For the nonlinear behavior of the soil, instead of using average stiffness a confining stress dependent stiffness for primary loading

path termed as E_{50} is used, for which is difficult to determine experimentally, and is given as

$$E_{50} = E_{50}^{ref}\left(\frac{c\cos\emptyset' - \sigma_s'\sin\emptyset'}{c'\cos\emptyset' + p^{ref}\sin\emptyset'}\right)^m \quad (4)$$

Such that:
E_{50}^{ref} is a reference stiffness modulus for primary loading corresponding to the reference stress p^{ref}
(In FEM, p^{ref} = 100 kN/m^2).

Effective confining pressure σ_3 influences the stiffness parameter and the amount of the influence is controlled by the parameter termed as power m as seen in equations (4) and (5). The range for which is different for different soil types typically from 0.5 to 1 in different soil types with the values of 0.9–1 for the clay soils (Schanz et al., 1999).

In hardening soil model, the stress dependent modulus is different for primary loading and for unloading and reloading stress paths. The stress dependent stiffness modulus for the unloading and reloading stress path is calculated as:

$$E_{ur} = E_{ur}^{ref}\left(\frac{c'\cos\emptyset' - \sigma_3\sin\emptyset'}{c'\cos\emptyset' + p^{ref}\sin\emptyset'}\right)^m \quad (5)$$

where:
E_{ur}^{ref} is a reference stiffness modulus for unloading/reloading corresponding to the reference stress p^{ref}. (In FEM, p^{ref} = 100 kN/m^2 and E_{ur}^{ref} equal to $3E_{50}^{ref}$).

3. METHODOLOGY

This section provides an overview of the methods employed for the analysis and presents the research findings. A visual representation of the entire process, exemplified by the flow chart in Figure 3.1, succinctly illustrates the sequence of steps.

The research unfolded through distinct stages:

a. Literature Review and Data Acquisition: This initial phase aimed to collect pertinent data essential for input into the Finite Element (FE) program. It encompassed acquiring parameters for silty sandy soil and conducting a literature analysis to identify correlations facilitating the preparation of collected data for input. Additionally, it involved a brief review of literature related to comparable earlier research.

b. Processing of Data for Input: All data gathered in step a underwent comprehensive processing, considering both mathematical and empirical relationships sourced from various books and literature. The objective was to meticulously prepare the data for subsequent modeling.

c. Input Data: To model the problem within the FE software, data from publications and literature analyzed in step b were amalgamated with additional relevant information derived through mathematical and empirical relationships.

d. Model Execution: A parametric exploration ensued, employing multiple numerical models created with consideration for various variables.

e. Output Data: Following the successful execution of the model in the FE program, output data were systematically collected, encompassing crucial parameters such as the soil's ultimate carrying capacity, settlement, deformation, and stress.

f. Processing of Output Data: This phase involved organizing and processing all outputs from step e, ensuring presentability and incorporating necessary verification for result validation. The outcomes were then compiled and compared with various parametric results.

The comprehensive methodology, from literature review to result validation, is encapsulated in the outlined stages, providing a clear understanding of the research process and its outcomes.

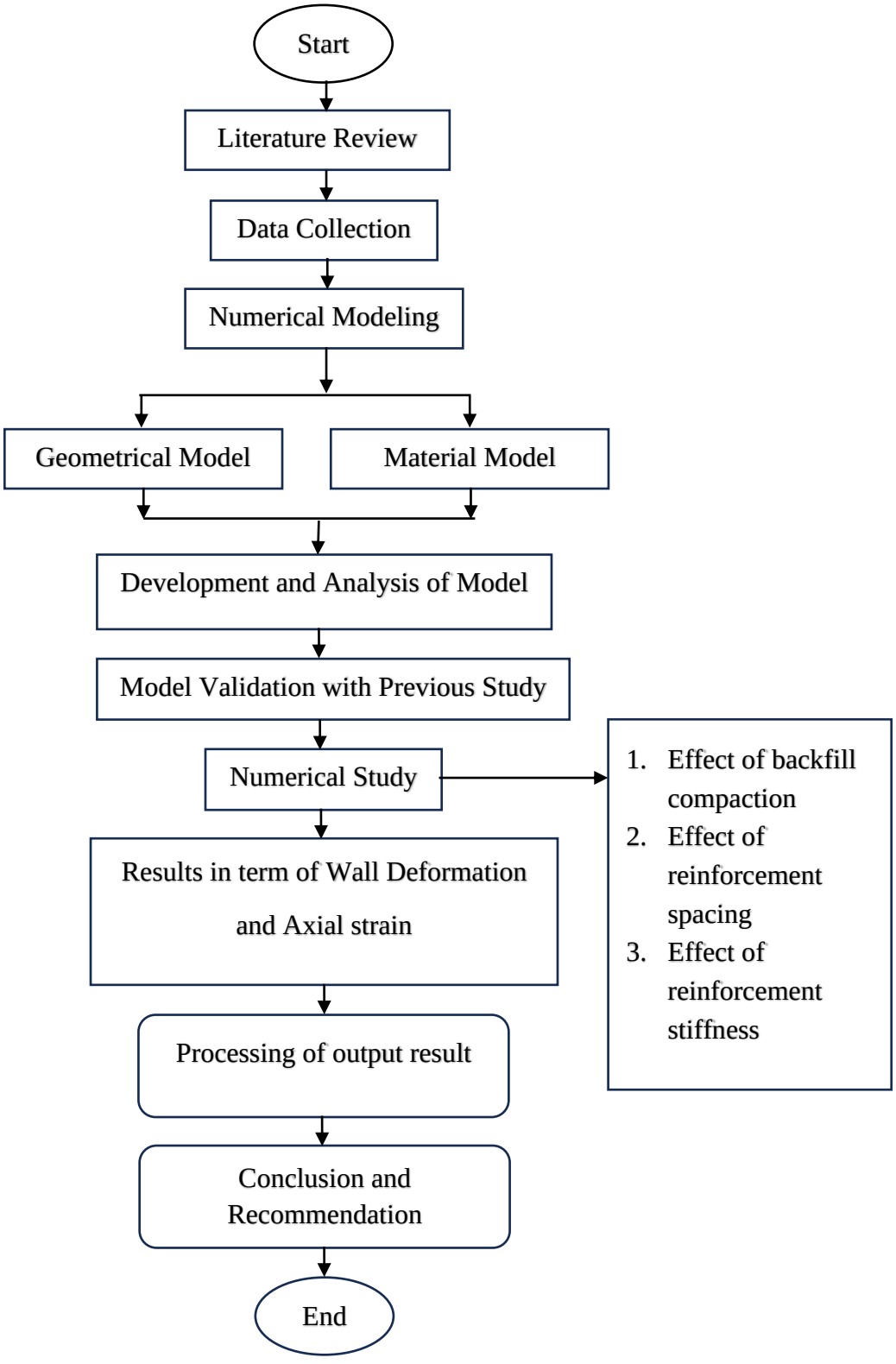

Figure 3.1 Employed Methodology

3.1. Literature Review of Previous Study:

3.1.1. Physical test wall model

Following figure describe the geometry and instrumentation layout of the physical test wall conducted by (Hatami & Bathurst, 2005).

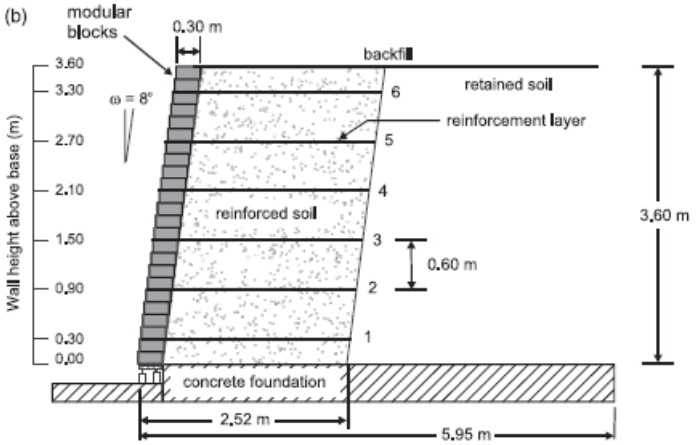

Figure 3.2 Schematic Diagram of the full-scale model (Hatami & Bathurst, 2005)

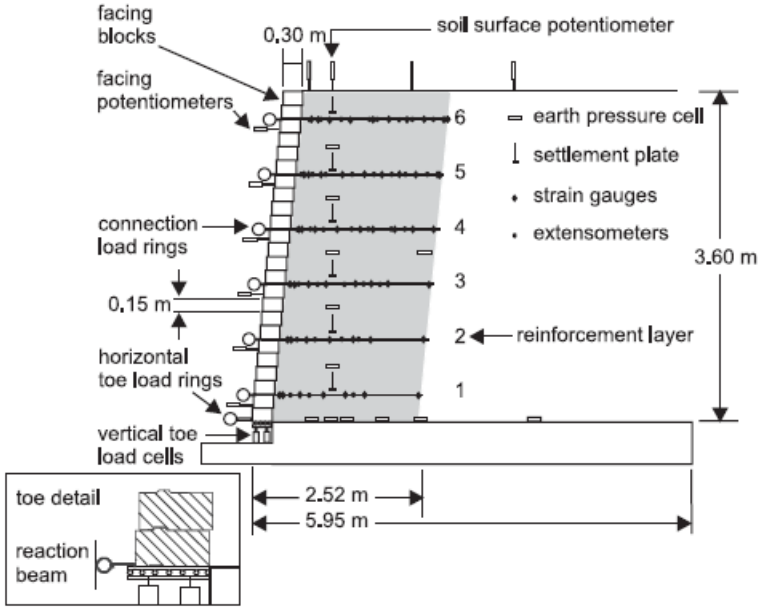

Figure 3.3 Test configuration and instrumentation (Hatami & Bathurst, 2005)

3.1.1.1. Numerical model

Previously, a finite difference model was developed to predict the response of geosynthetic-reinforced structure in which the backfill and modular block were modelled as continuum zones while the reinforcements were modelled as cable element (Hatami & Bathurst, 2005). The study compared the predicted wall response results

from the plane-strain numerical models with the measured responses of three 3.6 m high test walls constructed with sand backfill and different geogrid reinforcement stiffness and spacing. The numerical simulation was carried out using the finite-difference-based program, FLAC in which a homogeneous, isotropic, nonlinear elastic–plastic material with Mohr–Coulomb failure criterion and dilation angle (non-associated flow rule) model was used to model the compacted backfill soil. A set of guidelines for requiring soil backfill compaction was supplied by the study. Throughout the wall construction simulation, a transient 8 kPa vertical pressure was applied to the backfill surface at each stage. The study found that, for strains of less than 1.5%, a basic elastic–plastic soil model can accurately predict wall deformation, footing reaction response, and peak strain values in reinforcement layers—as long as the constant elastic modulus and Poisson's ratio for the sand backfill soil are chosen appropriately (Hatami & Bathurst, 2005). The linear elastic-plastic model used was shown to predict a contiguous zone of plasticity through the reinforced soil zone, which was inconsistent with measured results. It was also determined that the selection of an appropriate single-value elastic modulus is problematic due to the stress level dependency of granular soils. Nevertheless, nonlinear elastic-plastic soil models were found to give a better fit to the measured data. Hence, by using the parameters available in literatures, the backfill soil model was modelled using non-linear constitutive model termed as hardening soil model.

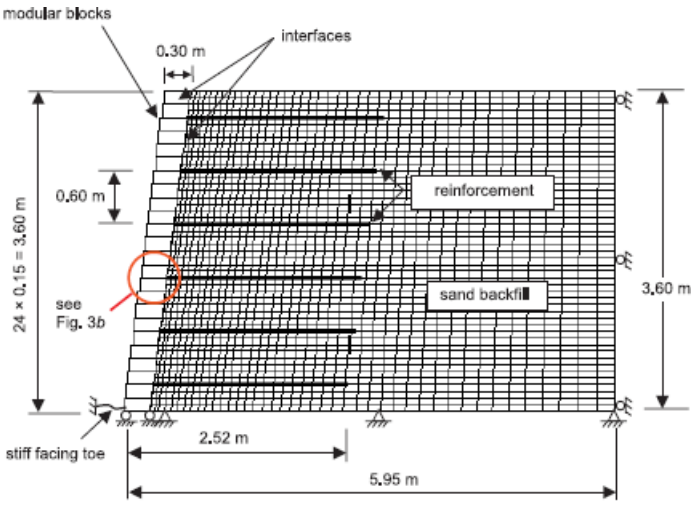

Figure 3.4 Numerical model based on FDM code adopted by (Hatami & Bathurst, 2005)

3.1.1.2. Geometry Modelling

The geometric modeling approach employed in this study mirrors that of (Hatami & Bathurst, 2005), encompassing dimensions as a key aspect of geometric properties. Figure 3.5 illustrates the 2D FEM geometric model adopted in this investigation. The wall's height was 3.6 m, featuring batter angle of facing as eight degrees from the vertical. The length of the backfill along the cross section was of six meters. The wall consists of a biaxial polypropylene geogrid of length 2.52 m long, having the vertical spacing of reinforcement as 0.6m. The facing block was of modular units comprised of solid masonry blocks, incorporating a shear key of continuous nature, dimensioning 300 mm length, 150 mm height, and 200 mm width.

In both x and y directions, fixed boundary condition was set on the bottom boundary of the model. The physical model included horizontal steel rollers beneath the toe, providing vertical fixity. To replicate this roller effect, the numerical analysis assumed vertical fixity below the toe. Additionally, a horizontal load cell ring positioned on the of the footing offered horizontal fixity and facilitated the measurement of horizontal toe reactions. The impact of the horizontal load ring, a horizontal fixed-end anchor was emulated with a 4000 kPa axial stiffness was placed on the toe, following the recommendation of (Hatami & Bathurst, 2005).

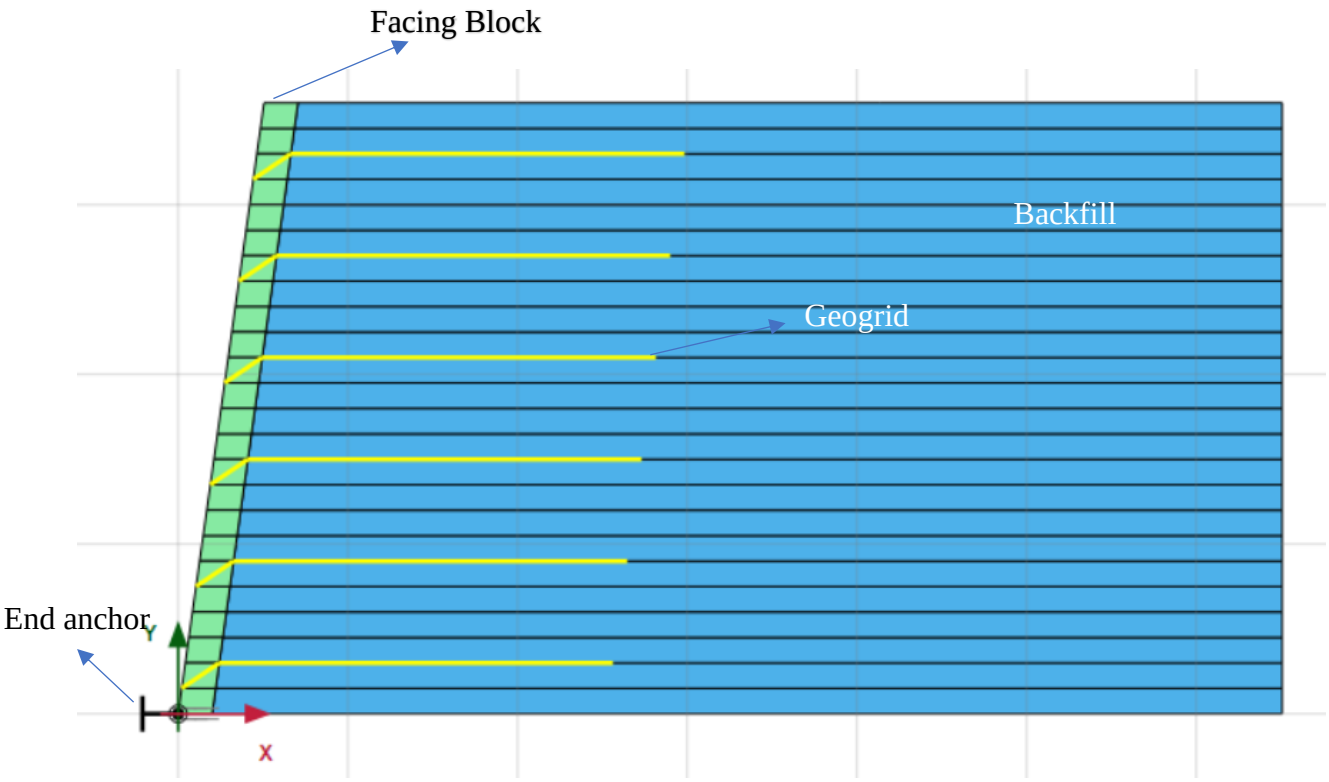

Figure 3.5 Finite Element Model developed in this study

3.1.1.3. Soil model and input parameters

(Hatami & Bathurst, 2005) propose the utilization of soil stiffness and strength parameters derived from plane-strain tests. The results of compression tests conducted under plane-strain conditions, along with the corresponding hyperbolas estimated at different normal pressures of increasing normal pressure. A favorable alignment is observed for confining pressures of 20 kPa and 30 kPa, particularly within the strain range of 0% to 1.5%. Anticipated confining pressures within the 3.6 m high model are not expected to exceed 30 kPa, and axial strain is projected to remain below 1.5% (Hatami and Bathurst, 2005).

Table 3.1 provides information on the properties of backfill sand including the angle of internal friction, angle of dilation, unit weight, value of cohesion adopted for numerical stability, reference stiffness modulus for primary loading and unloading and reloading stress paths and Poisson's ratio. For numerical stability such as to mitigate the minor local soil failures in model, a cohesion value of 5 kPa was assigned to the backfill soil as suggested in(Guler et al., 2012). The determination of hyperbolic model parameters for the validation model involves employing the results of plane-strain tests conducted on the backfill. As previously mentioned, the finite element model adopts 100 kPa as the default reference curve for the hyperbolic model.

Table 3.1 Backfill Soil Properties

Parameters	**Sand Backfill**
Material Model	Hardening Soil Model
Unit Weight γ (KN/m^3)	16.8
C′	5
$\phi°$	44
Ψ	11
E_{50}^{ref} (KN/m^2)	56667
E_{ur}^{ref} (KN/m^2)	=3* E_{50}^{ref} (KN/m^2) Default Setting
m	0.5
υ_{ur}	0.2
K_0^{nc}	0.3035
R_f	0.9
R_{inter}	0.67

3.1.1.4. Modular blocks

Linear elastic model was used to simulate the solid masonry modular facing unit. The properties of facing modular unit consist of unit weight, stiffness modulus and Poisson's ratio as shown in Table 3.3. The shear key of continuous nature of the modular block offers the frictional resistance which was modelled using interface element in finite element analysis.

Table 3.2 Modular Block Property

Parameters	Facing Element
Material Model	Linear Elastic
Unit Weight γ (kN/m^3)	21.8
Stiffness modulus, E (kN/m^2)	1×10^5
Poisson's ratio υ	0.15

3.1.1.5. Geogrid

The modeling of the extruded biaxial polypropylene geogrid reinforcement involved the use of infinite elastic elements. In the physical models, the connection linking the back of the modular facing element and geogrid was rigid for which, a representation of rigid connection was achieved by diagonally inserting geogrids into the modular blocks in finite element model used in this study.

For the reinforcement material, a single axial elastic stiffness value was adopted. Following the suggestion of (Hatami & Bathurst, 2005) to consider reduced axial stiffness values dependent on axial strain due to creep, the current model utilized a secant elastic modulus at 1.5% strain as an input parameter. This value corresponds to the maximum strain observed in the geogrids, as indicated by (Hatami & Bathurst, 2005). The secant stiffness Js(ε) for geogrids in Wall is expressed by (Hatami & Bathurst, 2005) as

$$J_s(\varepsilon) = \frac{T(\varepsilon)}{\varepsilon} = 119 - 1469\varepsilon \quad (6)$$

where $T(\varepsilon)$and ε are the axial load and axial strain respectively. The secant modulus for Wall was calculated as 97kN/m for the axial strain of 5%.

3.1.2. Field Model of GRS Bridge Abutment

Another use case of the GRS structure is its use as the bridge abutment. In this study, we modeled a plane strain finite element bridge abutment at Maree Micheal Bridge.

The plan and elevation view of the bridge is shown in Figure 3.6.

(a)

(b)

Figure 3.6 Maree Micheal Bridge a) Plan View b) Elevation View

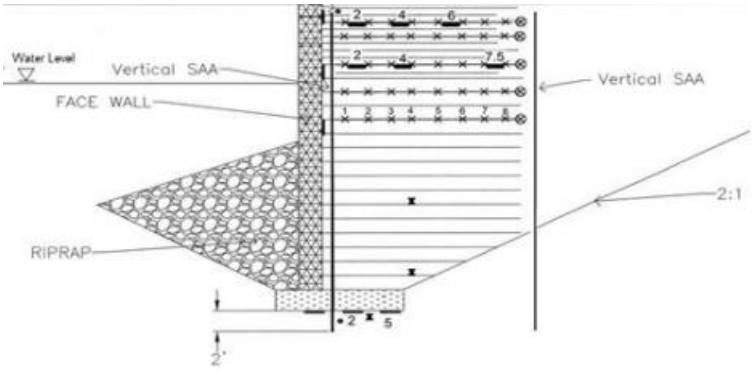

Figure 3.7 Instrumentation and Section of Maree Micheal Bridge

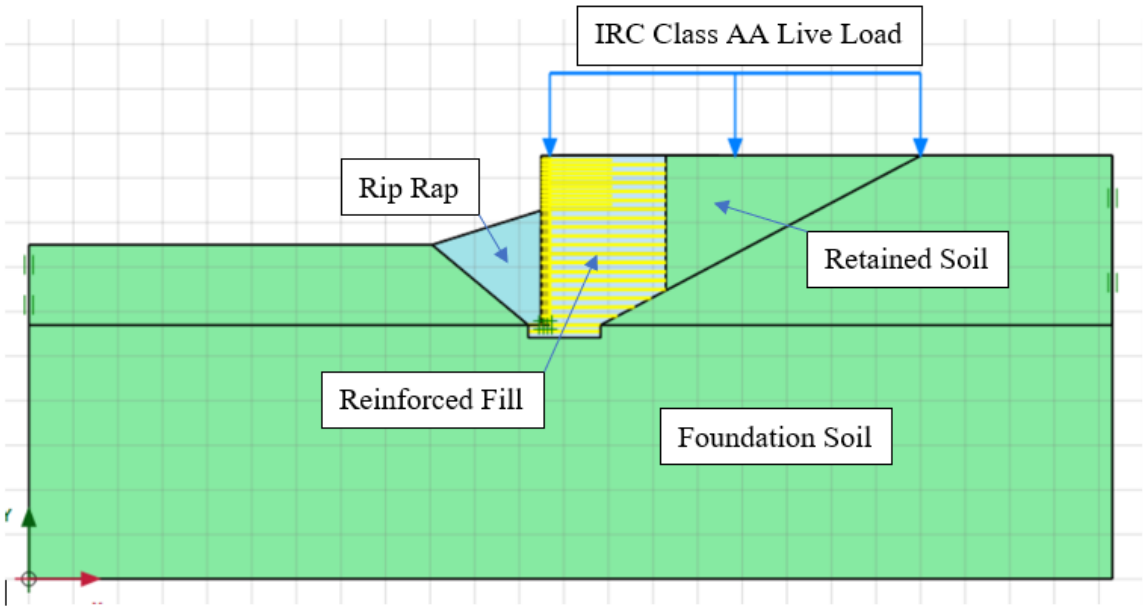

Figure 3.8 Plane Strain FE model of Maree Micheal Bridge

3.1.2.1. Finite Element Modeling

The plane strain finite element model to simulate the behavior of GRS Bridge abutment for different backfill compaction is presented in Figure 3.8 Plane Strain FE model of Maree Micheal Bridge. The finite element model developed is used for the numerical investigation which requires huge capital and time if performed on the full scale or prototype model. The field model was modeled as plane strain finite element model in previous studies.

The overall Geometric and material model properties are adopted from previous literatures. The material properties are show in Table 3.3, Table 3.4, Table 3.5, Table 3.6 and Table 3.7.

Table 3.3 Parameter for Modular Block

Parameters	**Modular Block**
Material Model	Linear Elastic
Dimensions	40.64×20.32×20.32
Unit Weight γ (kN/m^3)	21.8
Stiffness modulus, E (kN/m^2)	3×10^7
Poisson's ratio υ	0

Table 3.4 Parameter for backfill

Parameters	**Sand Backfill**
Material Model	Hardening Soil Model
Dry Unit Weight γd (KN/m^3)	18 kN/m /m^3
wet unit weight, γt	19 kN/m /m3
C′	20
ϕ°	51
Ψ	21
E_{50}^{ref} (KN/m^2)	34,000
E_{ur}^{ref} (KN/m^2)	=3* E_{50}^{ref} (KN/m^2) Default Setting
E_{oed}^{ref} (KN/m^2)	26,400
m	0.5
υ_{ur}	0.2
K_0^{nc}	0.3035
R_f	0.9
R_{inter}	0.67

Table 3.5 Parameter for Foundation Soil

Parameters	**Foundation Soil**
Material Model	Mohr-Coulomb model
Dry Unit Weight γd (KN/m^3)	15.2 kN/m /m^3
wet unit weight, γt	18.65 kN/m /m3
C′ (kPa)	17.7
ϕ°	27

Table 3.6 Parameter for Rip Rap

Parameters	**Rip Rap**
Material Model	**Linear Elastic**
Dimensions	40.64×20.32×20.32
Unit Weight γ (kN/m^3)	22
Stiffness modulus, E (kN/m^2)	50×10^3
Poisson's ratio υ	0.25

Table 3.7 Parameter for Geotextile

Category	**Description**
Geotextile	Linear elastic perfectly plastic model; Vertical spacing of 0.2m; and reinforcement axial stiffness 0f 600 kN/m.

A fixed boundary condition was implemented at the bottom of the Finite Element (FE) model, while roller boundary conditions were utilized on both sides. The overall height of the Geosynthetic-Reinforced Soil- Bridge Abutment (GRS-BA) wall measuring eight meters from the top of the Reinforced Soil Foundation (RSF). This height was

discretized into twenty layers to replicate the actual field construction process, employing the staged construction mode in PLAXIS 2D 2016. This mode facilitates the simulation of construction and excavation phases.

To emulate soil compaction during the staged construction process, a distribution load of 63 and 120 kPa (conducted for parametric analysis) was applied according to the type two compaction method; i.e, compaction load at the top and bottom of each soil layer. This load accounts for the induced stress on the backfill soil due to compaction, following the methodology introduced by (Mirmoradi & Ehrlich, 2015) .

4. RESULTS AND DISCUSSIONS

4.1. Experimental Model

After defining the model property as plain strain, geometric model was prepared and applicable model property and constitutive model was employed. The staged construction procedure was employed for the construction of the wall, where soil layers of 0.15 m thickness was placed in stage by stage method. A vertical load throughout the soil layer surface on each staged construction was applied to simulate the backfill compaction. For the study, two methodologies were employed: one with UDL at top and bottom simulating backfill compaction as described by(Mirmoradi & Ehrlich, 2018) and another with the UDL at top only. The load was removed before the placement of next layer. The reinforcement was activated after placement of immediate above layer.

4.1.1. Validation of Model Results

Here for the validation purpose, the predicted toe reactions, vertical foundation pressures and wall facing displacements from this study were compared with the full-scale experimental model and finite difference method

4.1.1.1. Toe Reactions

The load at fixed end anchor at each stage was obtained from the model and following plot was obtained.

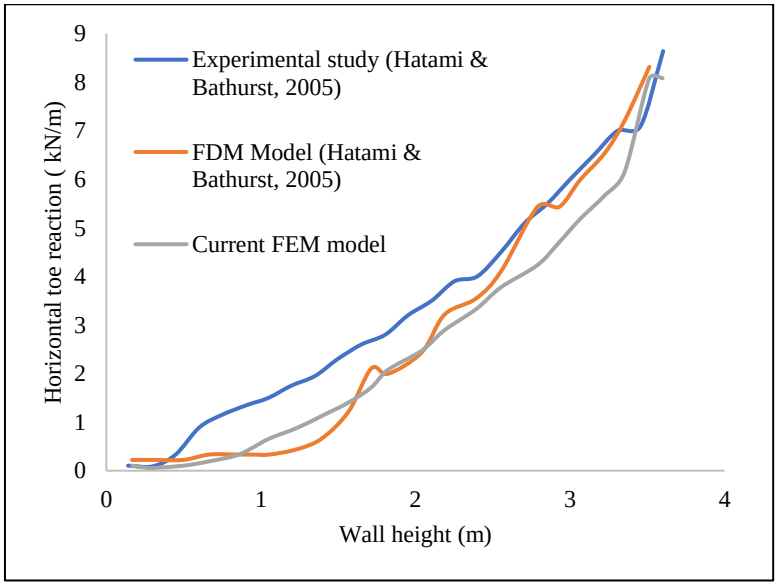

Figure 4.1 Comparisons of footing load at toe of wall

4.1.1.2. Vertical foundation pressures

The vertical foundation pressure was found at the bottom of the wall at footing wall behind the facing block.

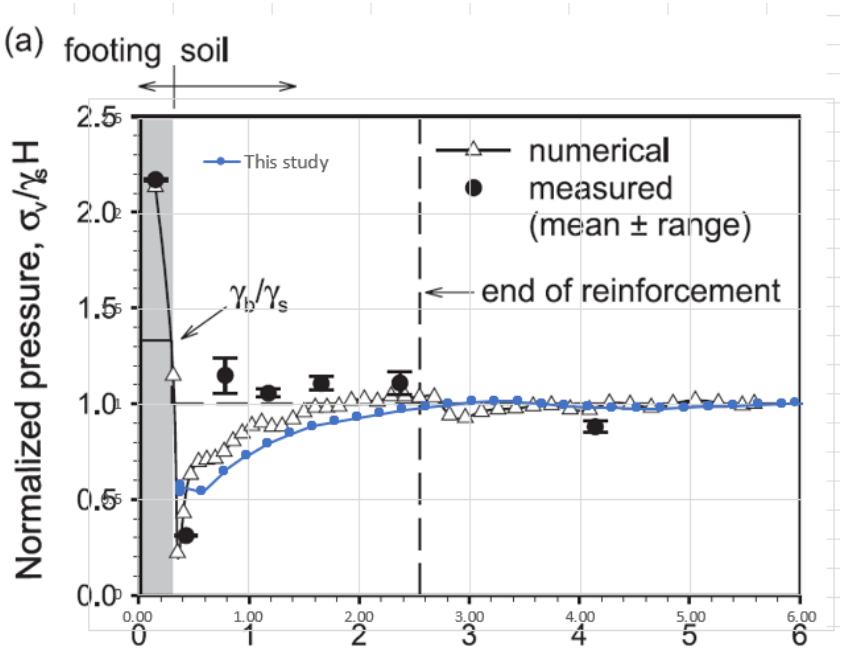

Figure 4.2 Comparisons of foundation soil pressure

4.1.1.3. Horizontal facing displacements

The lateral wall displacement observed at several instrument locations is depicted in the image. In the finite element analysis, the values correspond to the end of the construction phase. The measured values obtained from the full-scale test models were compared with these values. (Hatami & Bathurst, 2005) clarified that because the instrumentation recorded the amount of the lateral displacement value from the time of instrument insertion until the completion of construction, the measured facing displacements were not the real wall deformation profiles.

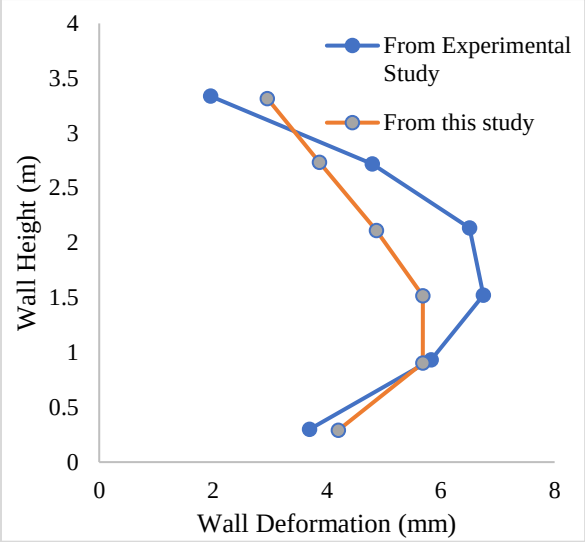

Figure 4.3 Horizontal Wall Displacement

4.2. Parametric Study

A parametric study was performed to investigate the lateral wall deformation on application of static surcharge load and on changing backfill compaction, the reinforcement spacing and stiffness. Experimental model used for validation in section 3.1.1.1 was used for the parametric study.

Further field model of fully-instrumented GRS bridge abutment at Maree Micheal Bridge in Louisiana was used for the finite element plane strain analysis and effect of the backfill compaction during service load is investigated in subsequent sections. The methodology of applying the compaction load for parametric analysis was based on the type II method as described in section 2.6.

4.2.1. Static Surcharge Load

Recent studies have indicated that the level of compaction for backfill soil can have important effects on the performance of GRS walls (Bathurst et al. 2009; Ehrlich et al. 2012; Mirmoradi and Ehrlich 2014). Numerical simulations were conducted for compaction stress (i.e., temporarily applied uniform surcharge stress) σ_c = 8, 16, 32 kPa, where σ_c = 8,16 and 32 kPa represent light, intermediate and heavy compactors, respectively. The following table shows the cases used in the study to determine the effect on compaction and surcharge at different stages.

Table 4.1 Cases used for study

Case	**1**	**2**	**3**	**4**	**5**	**6**	**7**	**8**	**9**	**10**	**11**	12
Surcharge Load (kPa)	8	16	20	32	8	16	20	32	8	16	20	32
Backfill Compaction (kPa)	8	8	8	8	16	16	16	16	32	32	32	32

The surcharge load applied at the top of the structure were selected as the values of backfill compaction load.

4.2.1.1. Effect on the lateral wall displacement

For two reinforcement axial stiffness, Figure 4.4 to Figure 4.11 show the effect of backfill compaction to the response of the structure. From these figures, it can be seen that as the heavy compaction is employed to the model, the lower the wall deformation in such model. Also, on decreasing the axial stiffness of the reinforcement, the deformation of the wall was increased.

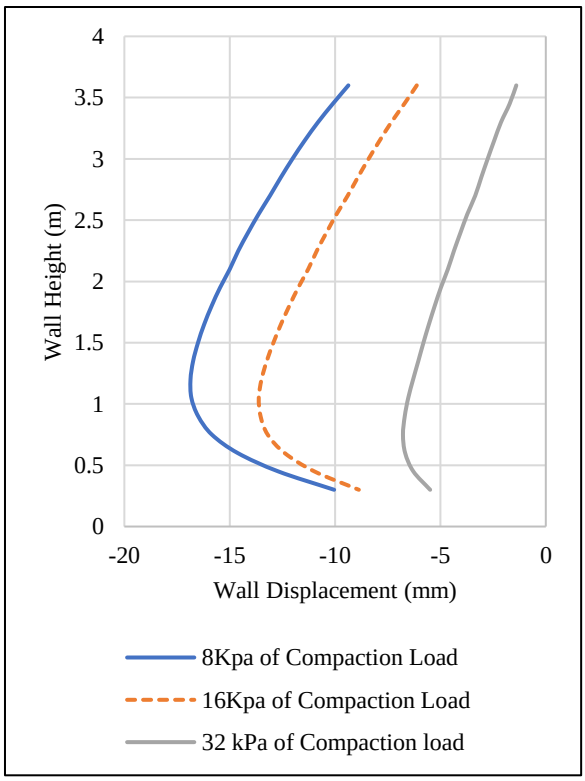

Figure 4.4 Lateral Wall displacement for 20 KPa of Surcharge (For 48.5 kN/m)

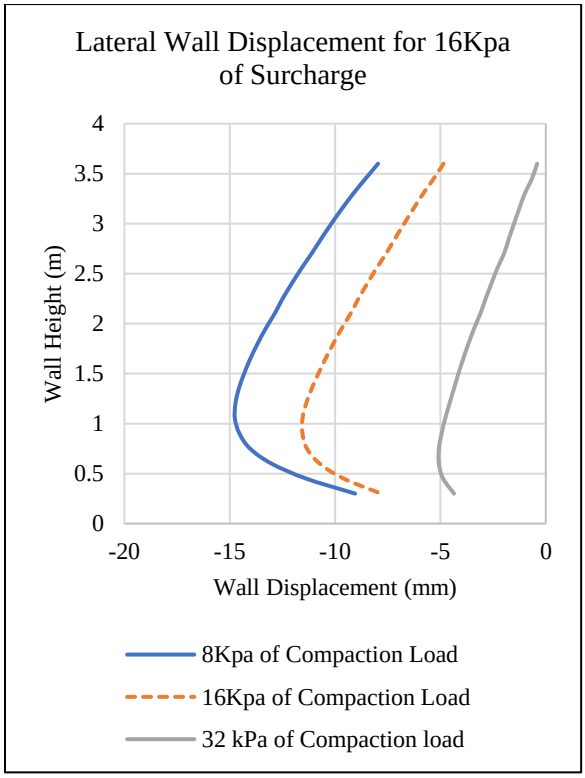

Figure 4.5 Lateral wall displacement for 16 kPa of surcharge (For 48.5 kN/m)

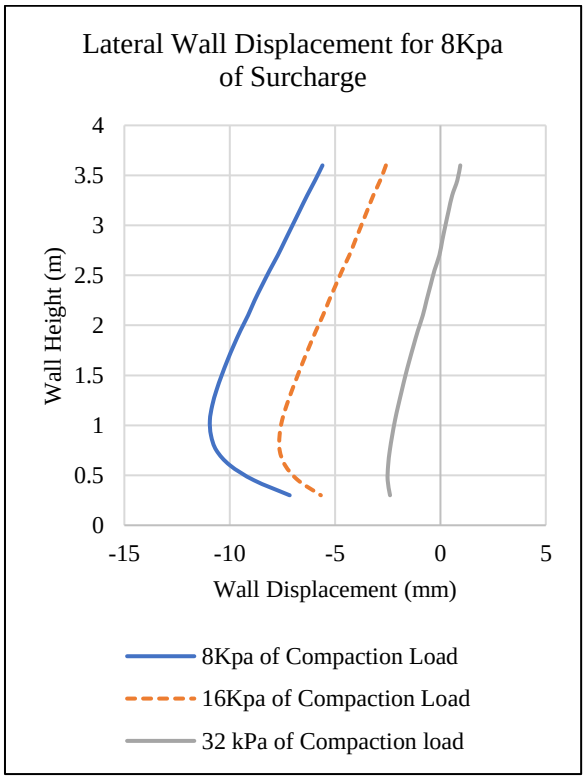

Figure 4.6 Lateral wall displacement for 8 kPa of surcharge (For 48.5 kN/m)

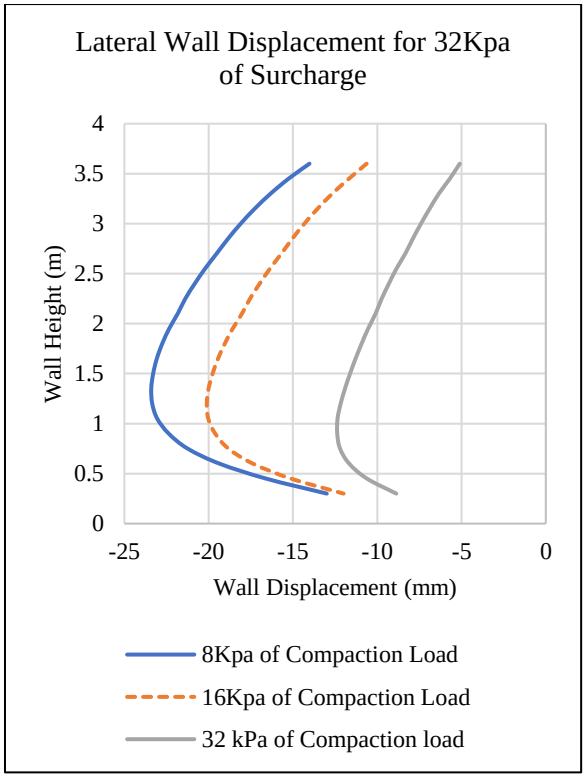

Figure 4.7 Lateral wall displacement for 32 kPa of surcharge (For 48.5 kN/m)

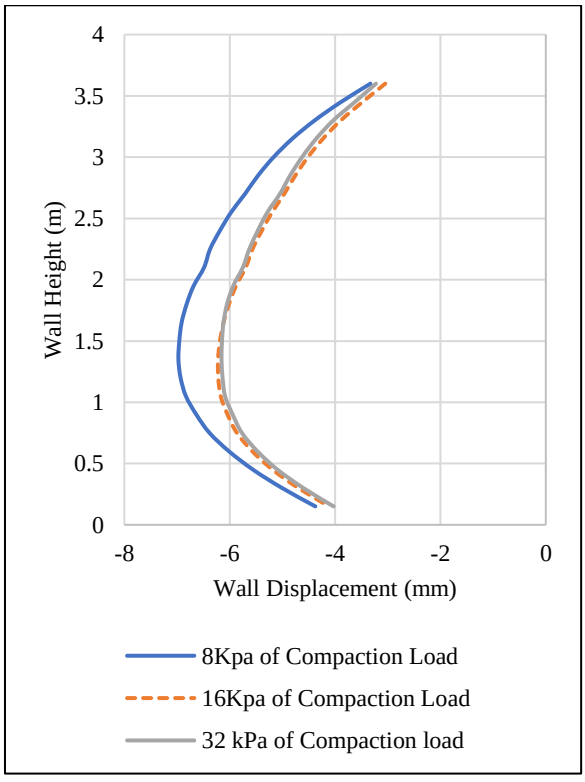

Figure 4.8 Lateral Wall Displacement for 20Kpa of Surcharge (For 97 kN/m)

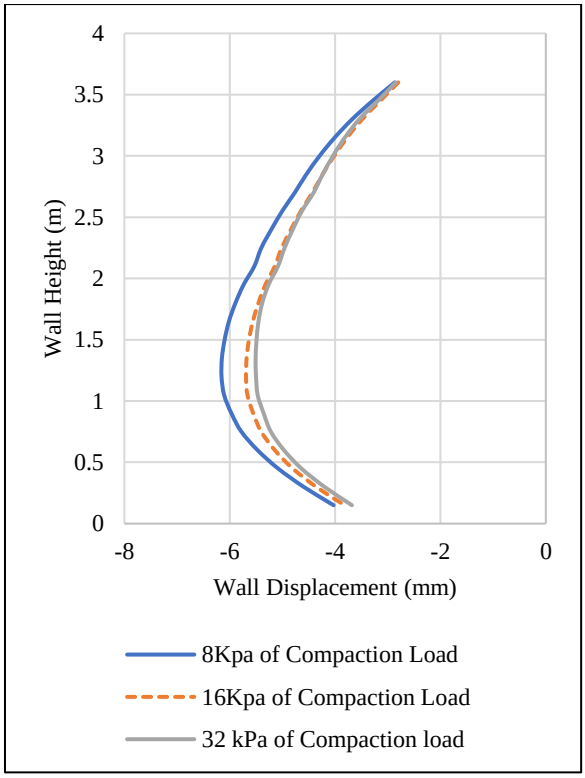

Figure 4.9 Lateral Wall Displacement for 16Kpa of Surcharge (For 97 kN/m)

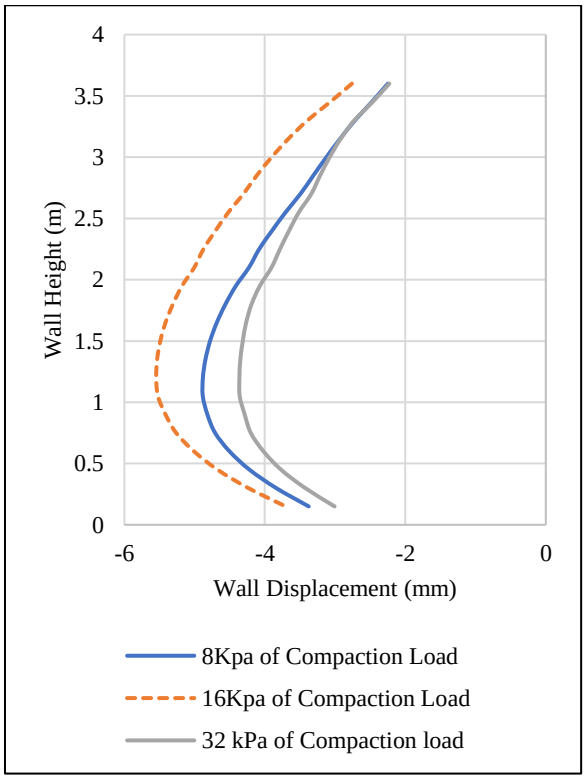

Figure 4.10 Lateral Wall Displacement for 8Kpa of Surcharge (For 97 kN/m)

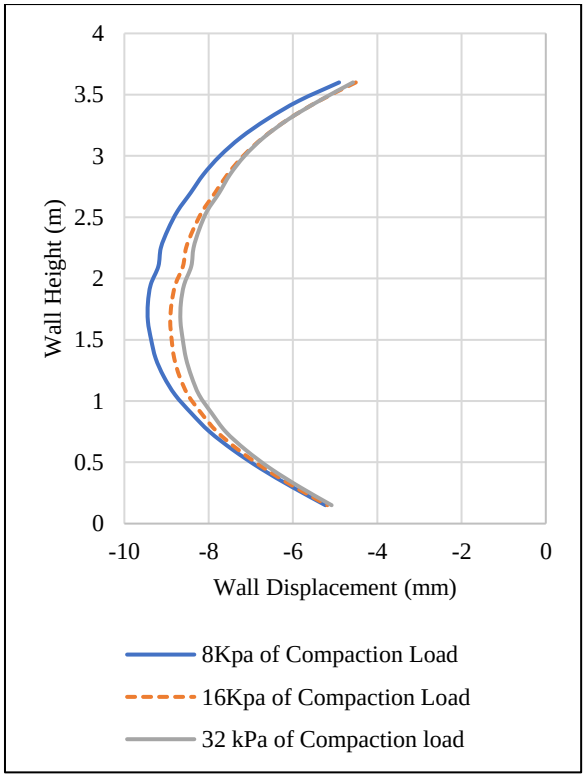

Figure 4.11 Lateral Wall Displacement for 32Kpa of Surcharge (For 97 kN/m)

4.2.1.2. Effect on Axial Strain of Geogrid

The Figure 4.12-Figure 4.17 shows the axial strain on the different layers of the geogrid on the application of the heavy surcharge (32 kPa). In upper layers of the geogrid, it can be seen that on increasing the backfill compaction, the axial strain (%) decreases. However, not much difference has been seen in the lower layer of reinforcements. Here, the effect on axial strain is observed for the model with axial reinforcement strain of 97 kN/m.

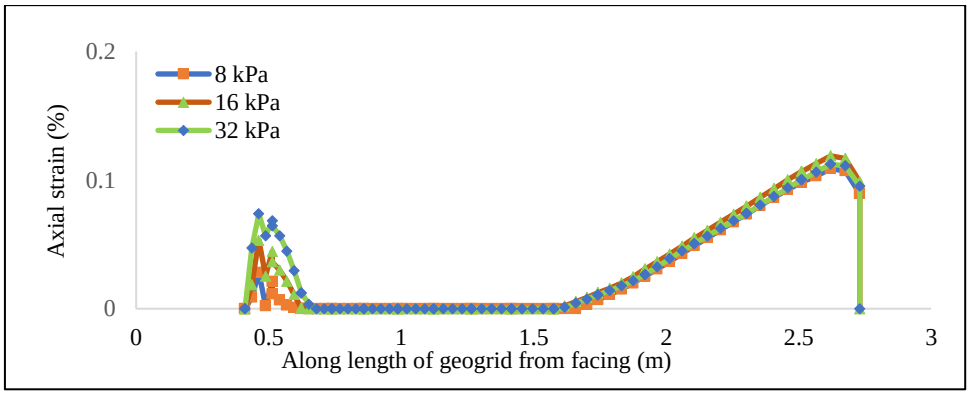

Figure 4.12 Axial Strain (%) in 1st layer

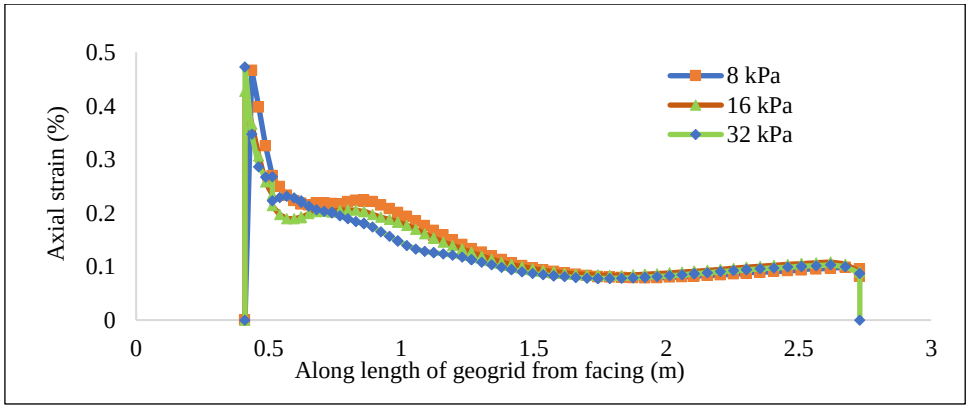

Figure 4.13 Axial Strain (%) in 2nd layer

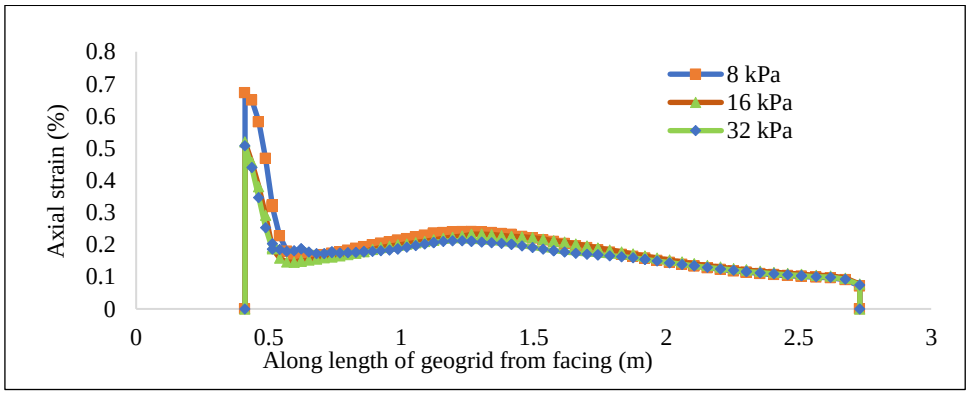

Figure 4.14 Axial Strain (%) in 3rd layer

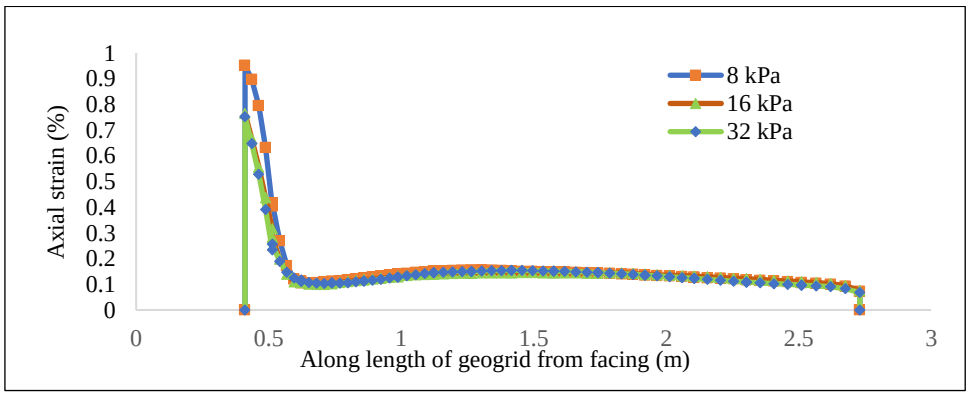

Figure 4.15 Axial Strain (%) in 4th layer

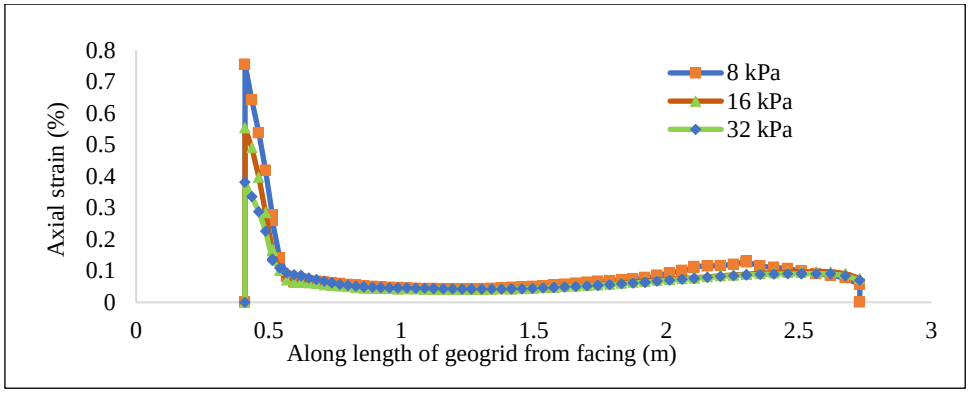

Figure 4.16 Axial Strain (%) in 5th layer

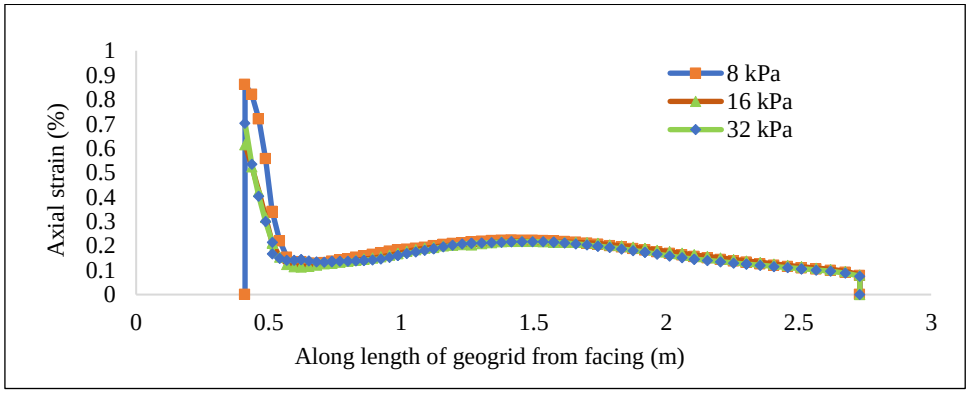

Figure 4.17 Axial Strain (%) in 6th layer

On the numerical model in which the effect of compaction was studied for different surcharge load, it was found that for the value of surcharge after construction, model with heavy compaction shows the more resistance to the lateral wall displacement than that with the light compaction which leads to the conclusion that the backfill compaction promotes the lock-in stress which in return increases the stiffness of soil mass as explained by others like (Ehrlich et al., 2012a),(Gui et al., 2020a), (Mirmoradi & Ehrlich, 2015). The following explains the finding of one of the authors supporting this claim.

(Ehrlich et al., 2012a) studied the effect of compaction and found that the lateral wall deformation was less for the physical model with heavy compaction during the surcharging than that for the physical model with light compaction which leads to conclusion that backfill compaction promotes the soil mass to undergo a kind of pre-consolidation state which leads the stiffer behavior of soil mass after end of construction, which is well explained by (Ehrlich et al., 2012a).

4.2.2. Effect of Reinforcement Spacing

For the experimental model, the vertical spacing of the reinforcement was changed and the effect of changing the reinforcement was investigated. Three different vertical spacing were studied for this study; vertical spacing of 0.15m, vertical spacing of 0.30m and vertical spacing of 0.60m. It was seen in all cases of surcharge and compaction; the deformation of the wall is less in the vertical spacing of 0.15m. The cases used for studying the effect of vertical spacing is shown in Figure 4.18.

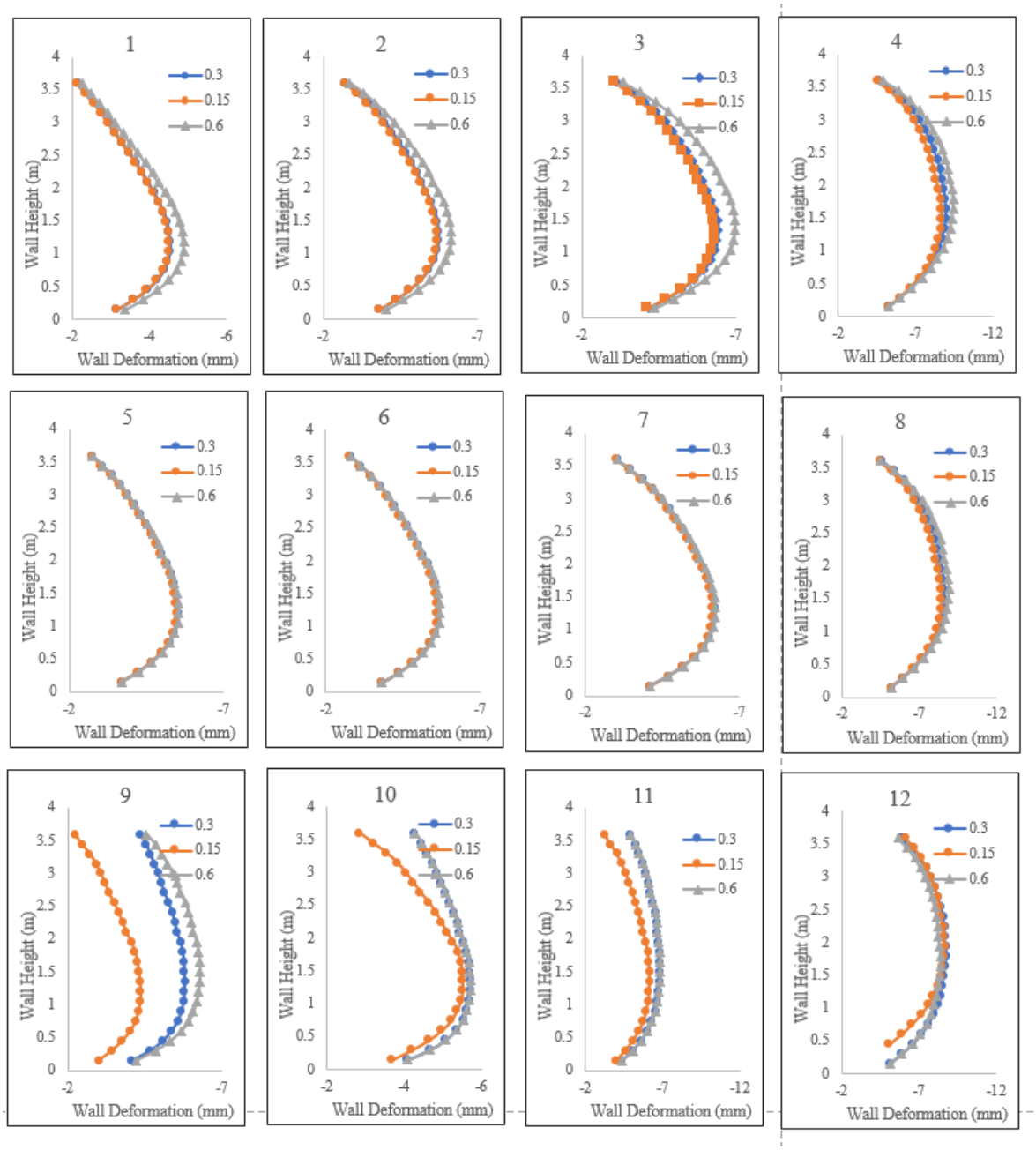

Figure 4.18 Effect of Reinforcement Spacing on wall deformation for cases defined in Table 2.1

4.2.3. Effect of Reinforcement Stiffness

Figure 27 ,28 and 29 shows the lateral wall deformation on application of heavy surcharge (32 kPa) on different geogrid axial stiffness. On decreasing the axial stiffness of the geogrid, the wall deformation has been increased. Here, the plain strain axial stiffness of the geogrid reinforcement used in the study are 48.5 kN/m and 97 kN/m.

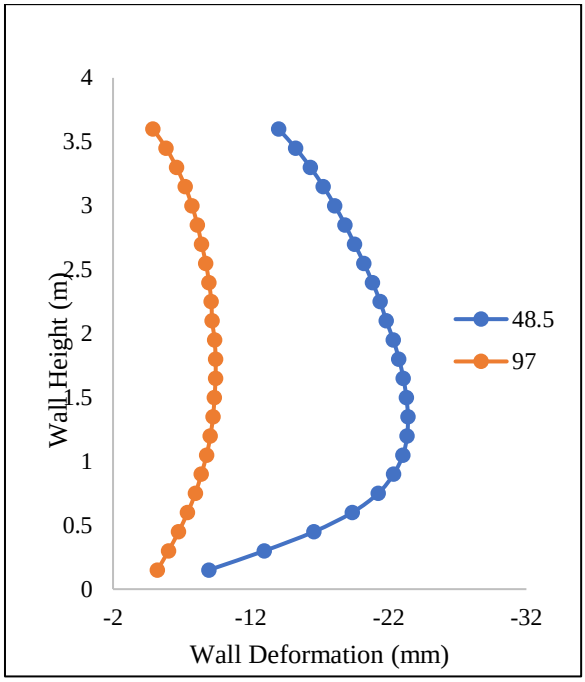

Figure 4.19 Lateral Wall Deformation for light compaction (8 kPa)

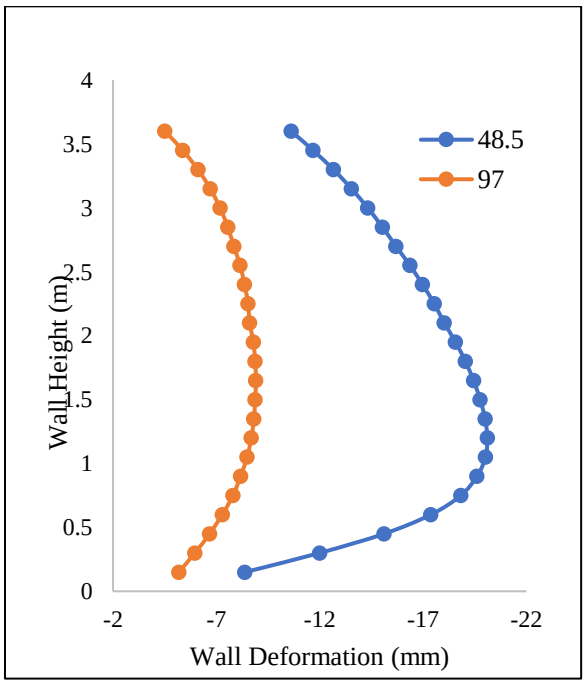

Figure 4.20 Lateral Wall Deformation for moderate compaction (16 kPa)

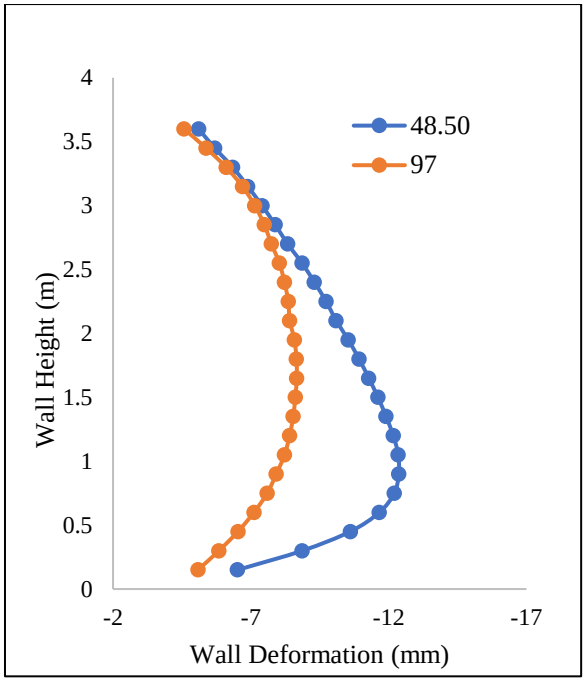

Figure 4.21 Lateral Wall Deformation for heavy compaction (32 kPa)

4.2.4. Effect of Relative Density

The effect of the changing the properties of the backfill sand has been studied by changing the relative densities of the backfill. The model was same as used in previous section but the parameters of backfill has been changed. Here, the effect of relative density for heavy compaction (32 kPa) has been considered.

The relationship among the relative density and the related parameters of Hardening Soil Model is given by following relations (Brinkgreve et al., 2010).

$$\gamma_{unsat} = 15 + 4.0 \cdot \frac{\mathrm{RD}}{100} \quad (7)$$

$$\gamma_{sat} = 19 + 1.6 \cdot \frac{\mathrm{RD}}{100} \quad (8)$$

$$E_{oed} = 60000 \cdot \frac{\mathrm{RD}}{100} \quad (9)$$

$$E_{50} = 60000 \cdot \frac{\mathrm{RD}}{100} \quad (10)$$

$$E_{ur} = 180000 \cdot \frac{\mathrm{RD}}{100} \quad (11)$$

$$m = 0.7 - \frac{\mathrm{RD}}{320} \quad (12)$$

$$\phi = 28 + 12.5 \cdot \frac{\mathrm{RD}}{100} \quad (13)$$

$$\psi \quad = (-2) + 12.5 \cdot \frac{\mathrm{RD}}{100} \tag{14}$$

$$R_f \quad = 1 - \frac{\mathrm{RD}}{800} \tag{15}$$

Table 4.2 Parameters Used for Hardening Soil Model (Brinkgreve et al., 2010)

Parameters	**Symbol**	**Unit**	**Relative Density (RD): 50%**	**Relative Density (RD) : 40%**	**Remarks**
Unsaturated Unit Weight	γ_{unsat}	kN/m^3	17.00	16.60	
Saturated Unit Weight	γ_{sat}	kN/m^3	19.8	19.64	
Secant stiffness from oedometer test	E_{oed}	kN/m^3	30000	24000	
Secant stiffness from drained triaxial test	E_{50}^{ref}	kN/m^3	30000	24000	
Reference unloading/reloading stiffness	E_{ur}^{ref}	kN/m^3	90000	72000	
Exponential Power	m	-	0.54375	0.575	
Poisson's ratio	ν	-	0.2	0.2	
Frictional Angle	ϕ	^{o}	34.25	33	
Dilation Angle	ψ	-	4.25	3	
Failure Ratio	R_f	-	0.9375	0.95	
Cohesion	C	kN/m^2	10	10	For numerical stability

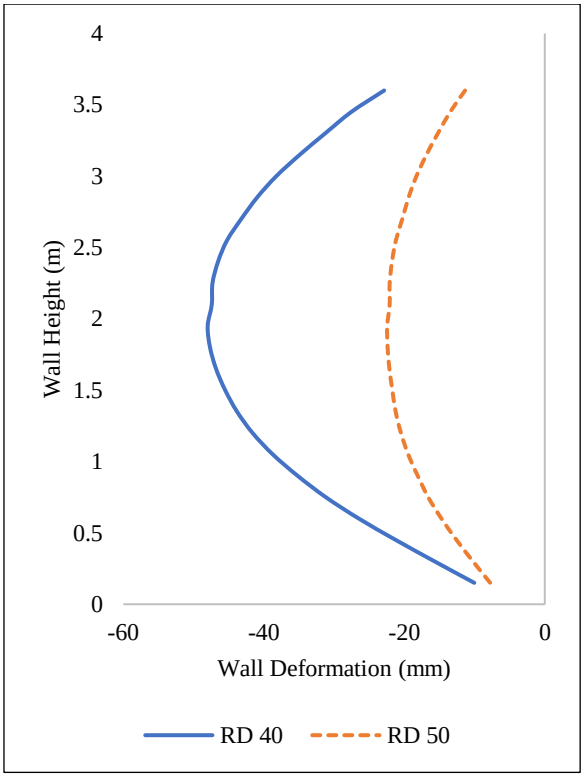

Figure 4.22 Wall Deformation for 32 kPa surcharge

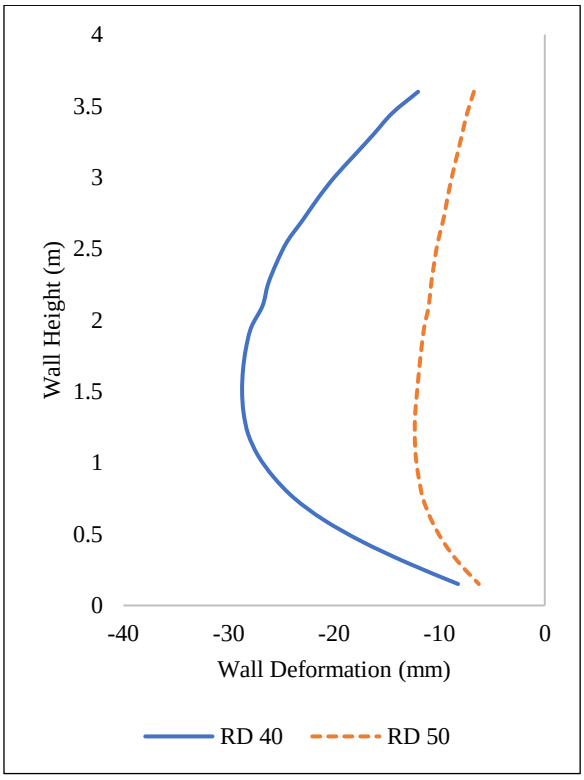

Figure 4.23 Wall Deformation for 8 kPa of Surcharge

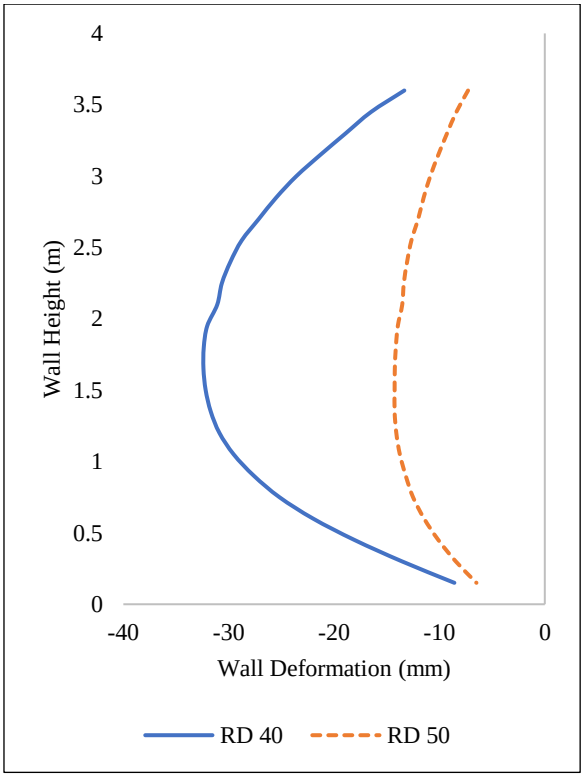

Figure 4.24 Wall Deformation for 16 kPa of surcharge

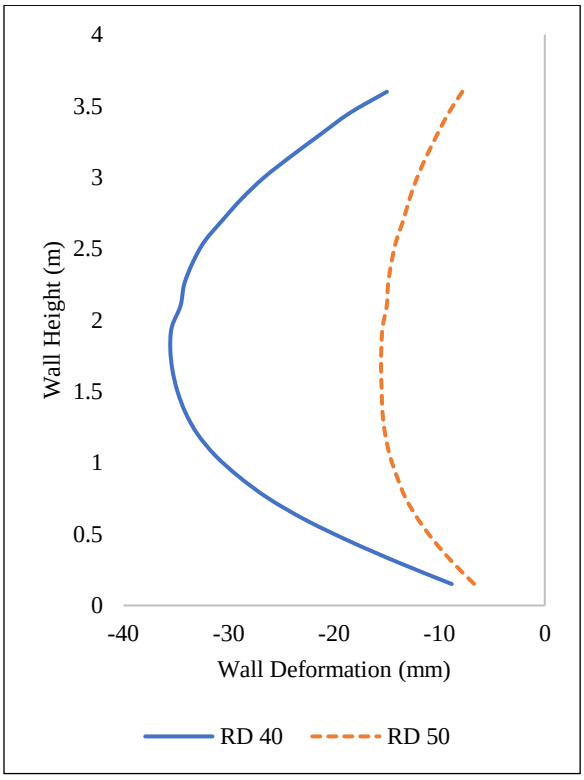

Figure 4.25 Wall Deformation for 20 kPa of Surcharge

4.3. Field Model

4.3.1. Effect of Compaction on Wall Deformation

Numerical simulations were conducted for compaction stress (i.e., temporarily applied uniform surcharge stress) σ_c = 63 and 120 kPa where, σ_c = 63 and 120 kPa represent light and heavy compactors, respectively.

For serviceability stage, live load representing the Class AA Tracked Loading of IRC Code-06,2014 was applied. The total weight of the Class AA Tracked load was of 700 KN with the contact length of 3.6m. The longitudinal view of the Class AA is shown in figure.

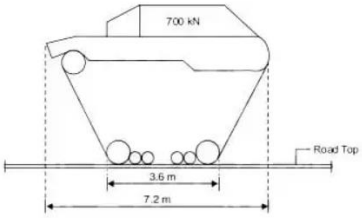

Figure 4.26 Longitudinal View of Class AA load as per IRC-06, 2014

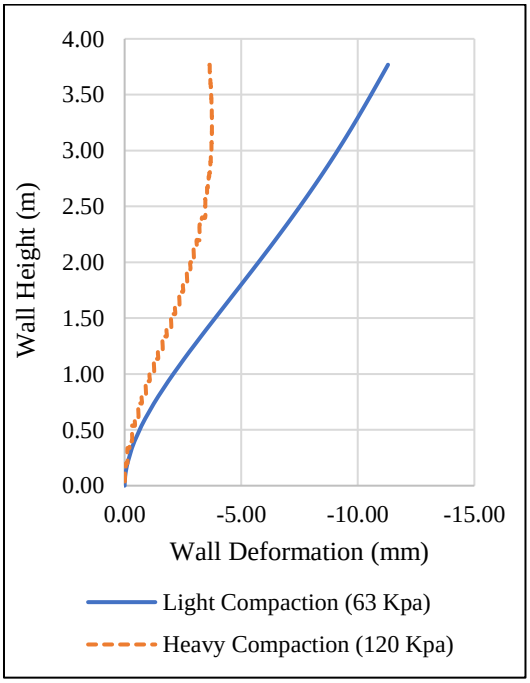

Figure 4.27 Effect of Backfill Compaction for Lateral Wall Deformation of GRS-BA

From Figure 4.27, it can be seen that with heavy compaction (120 kPa), the lateral wall deformation is less as compared to the light compaction (63 kPa) suggesting the increase of confinement and composite behavior due to compaction induced stress.

4.3.2. Effect of Compaction on Vertical Settlement

For vertical deformation, vertical deformation at level of 9.0m is plotted in Figure 4.28 and it is observed that the vertical deformation along the wall from the facing is less for the heavy compaction (120 kPa) as compared to the light compaction (63 kPa).

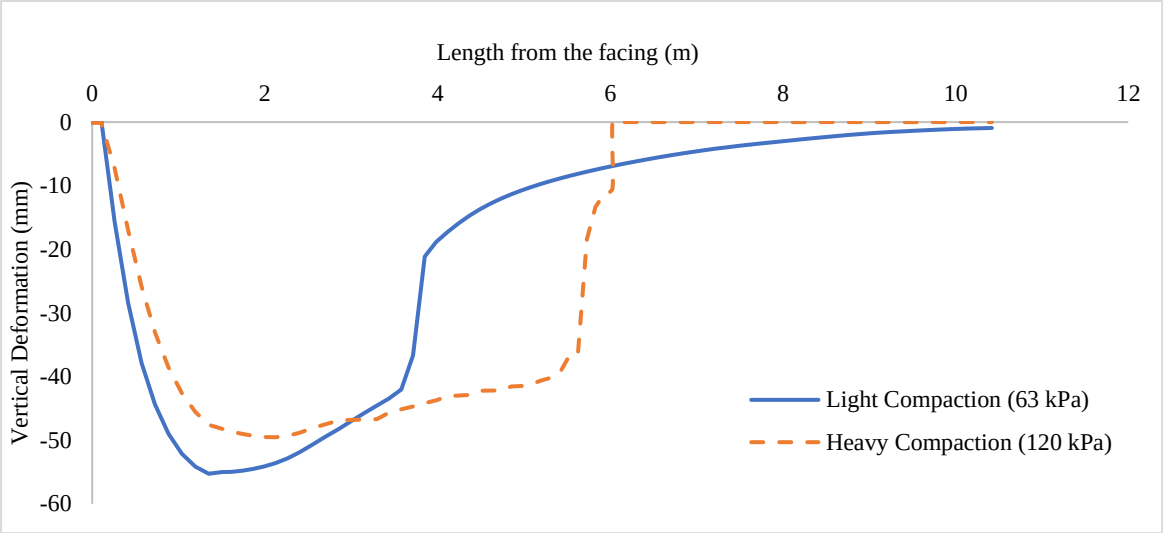

Figure 4.28 Effect of Backfill Compaction for Vertical Deformation of GRS-BA

4.3.3. Effect of Compaction on Axial Strain

In both uppermost layer (Figure 4.29) and bottommost layer (Figure 4.30) in the simulated field model, it was observed that the axial strain on the reinforcement is less for the model with heavy compaction (120 kPa) in comparison with model with light backfill compaction (63 kPa).

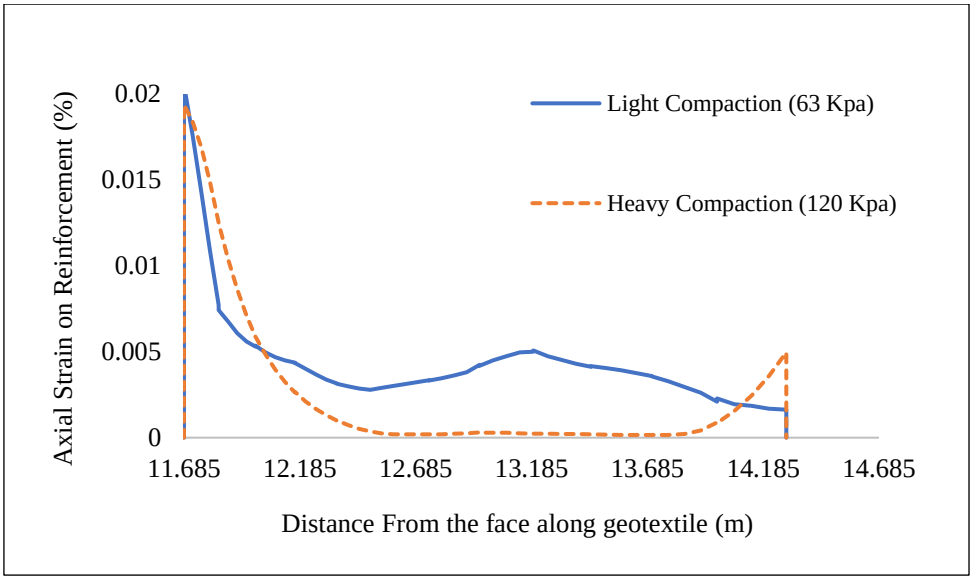

Figure 4.29 Axial Strain of Reinforcement on uppermost layer

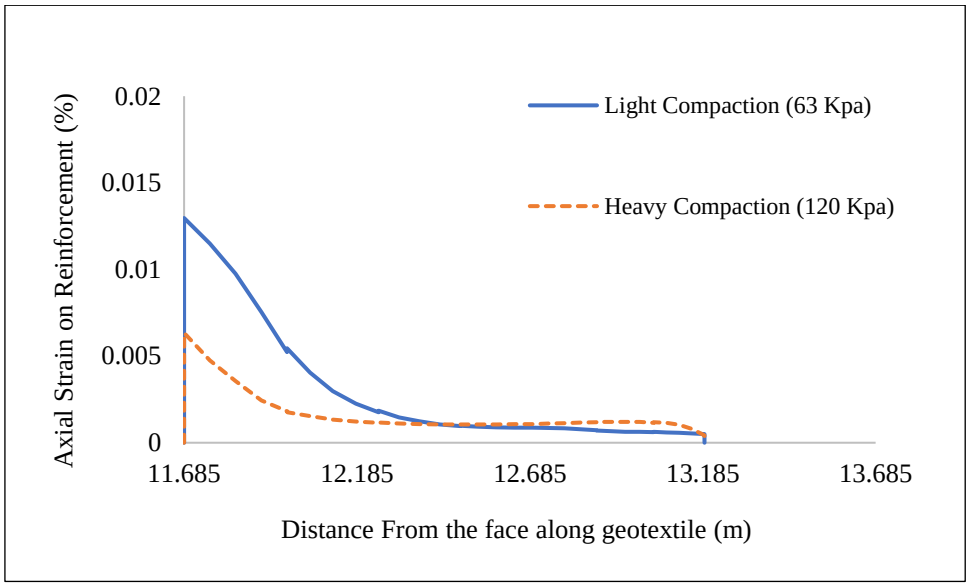

Figure 4.30 Axial Strain of Reinforcement on bottom most layer

5. CONCLUSION AND RECOMMENDATIONS

5.1. Conclusion

The numerical model's validation involved comparing its results to those obtained from a full-scale experiment within this study. Discrepancies in the outcomes can be attributed to disparities in field conditions and the numerical model itself. Additionally, variations in the vertical pressure results at the model's base stem from the difference in material behavior between hardening soil and the linear elastic modular block.

Furthermore, the compaction process near the wall face differed between the full-scale testing, which employed a light compactor, and this study, where compaction was uniformly applied throughout the entire soil continuum. This divergence in compaction methods may account for discrepancies observed in wall displacement and vertical soil pressure.

Regarding lateral wall deformation, experiments on differently compacted models subjected to various surcharge loads highlight how backfill compaction can enhance soil stiffness, consequently reducing deformities, a phenomenon discussed by several researchers.

Also, the parametric analysis was conducted to study the effect of the backfill compaction load on both geosynthetic reinforced wall and geosynthetic reinforced bridge abutment. It was found that the compaction plays significant role on resisting the lateral wall deformation. Also, with decreasing the vertical spacing of reinforcement, the lateral wall deformation was less as compared to the model with more vertical spacing. Regarding the stiffness of the reinforcement, the reinforcement having high axial stiffness resists the wall deformation as compared to the reinforcement having low axial stiffness. On the context of relative density of the backfill, for given compaction load, it can be seen that increased with the relative density resists the lateral wall deformations.

So, for the construction of the GRS structure as walls or bridges, it is important to note and supervise the compaction of the sandwiched backfill. Also, the compaction of the real field use should be such that the lateral and vertical deformations comply with the standards and codal provisions.

5.2. Recommendations

There are significant limits to this research, making it far from perfect. Following are some suggestions for upcoming work.:

- This study is only limited to the study of the geosynthetic reinforced wall in two-dimensional plane strain finite element model. Hence, further study can be carried out for the three-dimensional finite element model which accounts for the three- dimensional effect.
- The study is limited for the numerical model. Hence, further research can be carried out on the experimental and prototype model.
- The backfill material is compacted using a continuous uniformly distributed load which is the idealization of static and dynamic load imposed due to compactor. Hence, using a strip load or moving dynamic load, research can be performed to understand the long-term serviceability behavior of the structure subjected to the loads.
- The effect of horizontal toe resistance in experimental and the effect of the rip-rap, a counter measure against the scour, can be experimentally and numerically studied in further research.
- The geogrid is modelled as the infinite plain strain model in which effect of the aperture is considered in the property of the interface element between geogrid and the backfill compaction. So, in three-dimensional problem, geogrid can be modelled as the plate element with aperture which can provide actual wall response.

REFERENCES

Abdelouhab, A., Dias, D., & Freitag, N. (2011). Numerical analysis of the behaviour of mechanically stabilized earth walls reinforced with different types of strips. *Geotextiles and Geomembranes*, *29*(2), 116–129. https://doi.org/10.1016/j.geotexmem.2010.10.011

Abu-Farsakh, M., Ardah, A., & Voyiadjis, G. (2018a). 3D Finite element analysis of the geosynthetic reinforced soil-integrated bridge system (GRS-IBS) under different loading conditions. *Transportation Geotechnics*, *15*, 70–83. https://doi.org/10.1016/J.TRGEO.2018.04.002

Abu-Farsakh, M., Ardah, A., & Voyiadjis, G. (2018b). 3D Finite element analysis of the geosynthetic reinforced soil-integrated bridge system (GRS-IBS) under different loading conditions. *Transportation Geotechnics*, *15*, 70–83. https://doi.org/10.1016/j.trgeo.2018.04.002

Abu-Farsakh, M. Y., Ardah, A., & Voyiadjis, G. Z. (2019). Numerical parametric study to evaluate the performance of a Geosynthetic Reinforced Soil–Integrated Bridge System (GRS-IBS) under service loading. *Transportation Geotechnics*, *20*. https://doi.org/10.1016/j.trgeo.2019.04.001

Adams, M., Nicks, J., & others. (2018). *Design and construction guidelines for geosynthetic reinforced soil abutments and integrated bridge systems*.

Adams, M. T., Schlatter, W., & Stabile, T. (2007). *Geosynthetic Reinforced Soil Integrated Abutments at the Bowman Road Bridge in Defiance County, Ohio*.

Ardah, A., Abu-Farsakh, M., & Voyiadjis, G. (2017). Numerical evaluation of the performance of a Geosynthetic Reinforced Soil-Integrated Bridge System (GRS-IBS) under different loading conditions. *Geotextiles and Geomembranes*, *45*(6), 558–569. https://doi.org/10.1016/j.geotexmem.2017.07.005

Askari, M., Razeghi, H. R., & Mamaghanian, J. (2021). Numerical study of geosynthetic reinforced soil bridge abutment performance under static and seismic loading considering effects of bridge deck. *Geotextiles and Geomembranes*, *49*(5), 1339–1354. https://doi.org/10.1016/j.geotexmem.2021.05.007

Brinkgreve, R., Engin, E., & Engin, H. K. (2010, September). *Validation of empirical formulas to derive model parameters for sands*. https://doi.org/10.1201/b10551-25

Ehrlich, M., Mirmoradi, S. H., & Saramago, R. P. (2012a). Evaluation of the effect of compaction on the behavior of geosynthetic-reinforced soil walls. *Geotextiles and Geomembranes*, *34*, 108–115. https://doi.org/10.1016/J.GEOTEXMEM.2012.05.005

Ehrlich, M., Mirmoradi, S. H., & Saramago, R. P. (2012b). Evaluation of the effect of compaction on the behavior of geosynthetic-reinforced soil walls. *Geotextiles and Geomembranes*, *34*, 108–115. https://doi.org/10.1016/j.geotexmem.2012.05.005

Ehrlich, M., & Mitchell, J. K. (1994). WORKING STRESS DESIGN METHOD FOR REINFORCED SOIL WALLS. DISCUSSION AND CLOSURE. *Journal of Geotechnical Engineering*, *121*.

Gui, M., Phan, T., & Pham, T. (2020a). Impacts of compaction load and procedure on stress-deformation behaviors of a soil geosynthetic composite (SGC) mass-A case study. *Applied Sciences (Switzerland)*, *10*(18). https://doi.org/10.3390/APP10186339

Gui, M., Phan, T., & Pham, T. (2020b). Impacts of compaction load and procedure on stress-deformation behaviors of a soil geosynthetic composite (SGC) mass-A case study. *Applied Sciences (Switzerland)*, *10*(18). https://doi.org/10.3390/APP10186339

Guler, E., Cicek, E., Demirkan, M. M., & Hamderi, M. (2012). Numerical analysis of reinforced soil walls with granular and cohesive backfills under cyclic loads. *Bulletin of Earthquake Engineering*, *10*(3), 793–811. https://doi.org/10.1007/s10518-011-9322-y

Hatami, K., & Bathurst, R. J. (2005). Development and verification of a numerical model for the analysis of geosynthethic-reinforced soil segmental walls under working stress conditions. *Canadian Geotechnical Journal*, *42*(4), 1066–1085. https://doi.org/10.1139/t05-040

Huang, B., Bathurst, R. J., Hatami, K., & Asce, M. (n.d.). *Numerical Study of Reinforced Soil Segmental Walls Using Three Different Constitutive Soil Models*. https://doi.org/10.1061/ASCEGT.1943-5606.0000092

Jelušič, P., & Zlender, B. (2021). Experimental study of a geosynthetic-reinforced soil bridge abutment. *Geosynthetics International*, *28*. https://doi.org/10.1680/jgein.21.00022

Kondner, R. L., & Zelasko, J. S. (1963). *A Hyperbolic Stress-Strain Formulation of Sands*. 289–324.

Mirmoradi, S. H., & Ehrlich, M. (2015). Modeling of the compaction-induced stress on reinforced soil walls. *Geotextiles and Geomembranes*, *43*(1), 82–88. https://doi.org/https://doi.org/10.1016/j.geotexmem.2014.11.001

Mirmoradi, S. H., & Ehrlich, M. (2018). Experimental evaluation of the effect of compaction near facing on the behavior of GRS walls. *Geotextiles and Geomembranes*, *46*(5), 566–574. https://doi.org/10.1016/j.geotexmem.2018.04.010

Numerical modeling of a Geosynthetic Reinforced Soil-Integrated Bridge Systems (GRS-IBS) abutment subject to bridge loads. (n.d.). https://www.researchgate.net/publication/344026267

Rowe, R. K., & Skinner, G. D. (2001). Numerical analysis of geosynthetic reinforced retaining wall constructed on a layered soil foundation $. In *Geotextiles and Geomembranes* (Vol. 19).

Saghebfar, M., Abu-Farsakh, M., Ardah, A., Chen, Q., & Fernandez, B. A. (2017). Performance monitoring of Geosynthetic Reinforced Soil Integrated Bridge System (GRS-IBS) in Louisiana. *Geotextiles and Geomembranes*, *45*(2), 34–47. https://doi.org/10.1016/J.GEOTEXMEM.2016.11.004

Schanz, T., Vermeer, P., & Bonnier, P. (1999, September). Formulation and verification of the Hardening-Soil Model. *Beyond 2000 in Computational Geotechnics*.

Schlosser, F., & Long, N.-T. (1974). Recent Results of French Research on Reinforced Earth. *Journal of the Construction Division*, *100*(3), 223–237. https://doi.org/10.1061/JCCEAZ.0000429

Wu, J. T. H. (2019). Characteristics of Geosynthetic Reinforced Soil (GRS) Walls: an Overview of Field-Scale Experiments and Analytical Studies. *Transportation Infrastructure Geotechnology*, *6*(2), 138–163. https://doi.org/10.1007/s40515-019-00074-x

Wu, J. T. H., & Pham, T. Q. (2010). An analytical model for evaluation of compaction-induced stresses in a reinforced soil mass. *International Journal of Geotechnical Engineering*, *4*(4), 549–556. https://doi.org/10.3328/IJGE.2010.04.04.549-556

Wu, J. T. H., & Pham, T. Q. (2013). *Load-Carrying Capacity and Required Reinforcement Strength of Closely Spaced Soil-Geosynthetic Composites*. https://doi.org/10.1061/(ASCE)GT.1943

Wu, J. T. H., Yang, K.-H., Mohamed, S., Pham, T., & Chen, R.-H. (2014). Suppression of Soil Dilation—A Reinforcing Mechanism of Soil-Geosynthetic Composites. *Transportation Infrastructure Geotechnology*, *1*(1), 68–82. https://doi.org/10.1007/s40515-014-0003-6

Yang, Z. K. (1972). *Strength and deformation characteristics of reinforced sand*. https://api.semanticscholar.org/CorpusID:139057854

Zelenko, B. H., Alzamora, D., & Nicks, J. E. (2019). Deployment of the Geosynthetic Reinforced Soil (GRS) Integrated Bridge System (IBS) from 2011 to 2017. *Geo-Congress 2019: Earth Retaining Structures and Geosynthetics*, 140–150.

Zheng, Y., & Fox, P. J. (2017). Numerical Investigation of the Geosynthetic Reinforced Soil–Integrated Bridge System under Static Loading. *Journal of Geotechnical and Geoenvironmental Engineering*, *143*(6). https://doi.org/10.1061/(asce)gt.1943-5606.0001665

LIST OF PUBLICATIONS

Ghimire, S., & Yadav, S.K. (2023). Investigating the Influence of Compaction Load on Lateral Wall Deformation in Geosynthetic Reinforced Structures. 14th IOE Graduate Conference (Accepted)